

Highly Conductive Fluoropolymer Based Composite Ink for Printed Stretchable Electronics

by

Amit Kumar

A thesis submitted in the partial fulfillment of the requirements for the degree of

Master of science

in

MATERIALS ENGINEERING

Department of Chemical and Materials Engineering

University of Alberta

© Amit Kumar, 2017

Abstract

The recent development of stretchable electronics expands the scope of wearable and healthcare applications. This creates a high demand in stretchy conductor that can maintain conductivity at high strain conditions. Here, we describe a simple and novel fabrication way to achieve stretchable, 3D-printable and low-cost conductive composite ink. It can be favorable in printing the complex stretchable patterns with high conductivity. Such elastic ink is composed of silver(Ag) flakes, fluorine rubber, an organic solvent and dispersive agent. The dispersive agent must be compatible with the chosen fluorine rubber as it accounts for multiple roles in the composite which promotes compatibility between silver flakes and fluorine rubber and also affects the mechanical properties of the hosting fluoropolymers as well as adhesion properties of the composite. Based on experimental observations in our work, we discuss the exact role of the dispersive agent in the composite. The resulting composite exhibits high conductivity value of 8.49×10^4 S/m along with high reliability against repeated four stretching/releasing cycles. Interesting examples of transfer printing of the printed ink and its applications in working devices, such as conformal antennas and stretchable heater, are also showcased.

Keywords: flexible electronics, elastic conductive ink, dispersive agent, polymer composites, printed antennas

Preface

(Mandatory due to collaboration)

1. Chapter sections 1.1, 2.1, 3.2, 3.3,4.1 ,4.2 of this thesis is based on a manuscript for peer-reviewed publication as Amit Kumar, Hossein Saghlatoon, Thanh Giang La, Mohammad Mahdi Honari Kalateh, Hemant Charaya, Haitham Abu Damis, Pedram Mousavi, Hyun-Joong Chung “**A Highly Deformable Conductive Ink for Printed Antennas and Interconnects: Silver/Fluoropolymer Composite Amalgamated by Triethanolamine**”, to be submitted to **Flexible and Printed Electronics**. In this manuscript, I conceived ideas on materials with T.G.L. and H-J.C. I performed all the measurements of physicochemical properties and mechanical durability with contribution and guidance from T.G.L as shown in the chapter 3.2 and 3.3. All the data interpretation in chapter 2 and chapter 3 with advices from T.G.L and H.J.C. H.S., M.M.H., H.A.D., and P.M. conceptualized and characterized antennas. Simulation, antenna characterization and data interpretation in Chapter 4.2 are primarily done in Dr. Mousavi’s research group; I fabricated the antennas as shown in the chapter 4.1 with the help from T.G.L.

2. Chapters 4.3 of this thesis is based on manuscript for peer-reviewed publication as Thanh Giang La, Xinda Li, **Amit Kumar**, Yiyang Fu, Shu Yang, Hyun-Joong Chung “**Modulating Phase Transition Temperature of Tough Hydrogel Coating for Stretchable Smart Window Application**”, to be submitted to **Advanced materials**. I prepared the elastic ink and fabricated stretchable heater with helps of T-G.L. I also contributed to the smart window fabrication led by T-G.L.

Acknowledgements

First and foremost, I would like to thank my mentor and supervisor, Dr. Hyun-Joong Chung for his everlasting advice, support and encouragement for my research throughout the degree. More than two years I spent here passed like a breeze working under his excellent supervision. He has a unique way of explaining things and great sense of humor that makes me work with him more smoothly and comfortably. I thank him for being so kind with my numerous questions, technical queries and sloppy manuscripts. Apart from my research, he taught me about the time management, career goals and life outside the academics. I sincerely express my gratitude to him and I am deeply indebted to him for all his efforts and help.

I thank Dr. Thanh Giang La, for his help and guidance during my project. He had been a constant source of information for all the results and measurement queries. I would also like to thank Hemant Charaya and Xinda Li for helping me in understanding the chemistry part of the ink. I would highly like to thank Dr. Pedram Mousavi and his group for helping us in antenna designs and their measurements. I would also like to express my gratitude to Jiaxin, who helped me in learning the 3D printer in a perfect manner.

Finally, and most importantly I would like to express my gratitude to my parents, siblings and my friends for their love and care. They have always been a constant source of encouragement and supporting me throughout my entire life.

Table of Contents

Abstract

1. Introduction.....	1
1.1) Introductory overview of the thesis	1
1.2) 3D Printing Techniques.....	4
1.2.1) Fused Deposition Modeling (FDM).....	5
1.2.2) Stereo-lithography.....	7
1.2.3) Ink Jet Printing.....	8
2. Fabrication procedure of Ag elastic ink.....	10
2.1) Materials and methods.....	10
2.1.1) Materials.....	10
2.1.2) Preparation of highly conductive elastic ink.....	11
2.1.3) Role of TEA in the elastic ink solution and in the stretchable trace.....	12
2.2) Selection of substrate	14
2.3) nSyrpt 3Dn printer and its components.....	17
2.3.1) Printing procedres.....	18
2.3.2) Nozzle diameter.....	19
2.4) Drop Impact and Spreading Behavior.....	19
2.4.1) Rheology Control.....	21
2.4.2) Droplets phase behavior and Stability.....	22

2.4.3) Ink Drying.....	26
3. Characterization of ink properties.....	28
3.1) Characterization Techniques.....	28
3.2) Physicochemical properties of the ink.....	29
3.2.1) Viscosity measurement.....	29
3.2.2) Thermal stability of elastic ink and its components.....	31
3.2.3) Conductivity variation with silver content wt.%.....	32
3.2.4) Temperature effect on the resistance.....	34
3.3) Mechanical durability of the ink	35
3.3.1) Adhesion tests on various substrates.....	39
4. Applications using elastic ink.....	41
4.1) Schematics of elastic ink fabrication and the printing of stretchable traces onto elastomeric substrate for stretchable antenna fabrication.....	41
4.2) Conformal antennas.....	42
4.2.1) On-body loop antenna.....	43
4.2.2) WLAN stretchable antennas.....	44
4.2.3) Antennas measurement and results.....	46
4.2.4) Limitation of using Vector network analyzer (VNA).....	48
4.3) Stretchable Heater.....	49

4.3.1) Dimension and working.....	50
5. Conclusion.....	53
6.Future Work.....	56
7. List of References.....	57
Appendix 1 – Supplementary Data.....	61

List of Tables

Table 1: Properties of various substrates.....	15
Table 2: Conductivity measurements with Silver content wt.%.....	34
Table 3: Comparison study of various elastic ink	38
Table 4: Characteristics of the body tissues and layers. Reproduced with permission from[59]..	44

List of figures

Figure 1.1: Reduction of metal ions. Reproduced with the permission from [9-11].....	2
Figure 1.2: Composite based ink. Reproduced with the permission from [13-16]	3
Figure 1.3: Fused Deposition Modeling. Reproduced with the permission from [22].....	6
Figure 1.4: Extrusion AM process principle and schematic. Reproduced with permission [21]..	7
Figure 1.5: Schematic of stereolithography process. Reproduced with permission from [24].....	8
Figure 1.6: Schematic of Continuous mode- Inkjet printing and DOD printing. Reproduced with permission from [25].....	9
Figure 2.1: Chemical structure of the ink components.....	10
Figure 2.2: Steps for the preparation of 3D printable Ag elastic ink.....	12
Figure 2.3: Schematic based on the role of TEA in fluoropolymer based elastic ink.....	13
Figure 2.4: VHB 4910 3M Company	14
Figure 2.5: nScrypt 3Dn printer and its parts.....	17
Figure 2.6: Schematic illustration of the sequence of events that occurs after droplet impact on a substrate. Reproduced with permission from [40].....	20
Figure 2.7: Fluid regime properties in DOD. Reproduced with the permission from [40].....	25
Figure 2.8: Self-organization of solute during drop drying using marangoni flow. Reproduced with the permission from [51].....	27

Figure 3.1: Viscosity variation with shear rate.....	30
Figure 3.2: TGA of conductive ink and its components	32
Figure 3.3: Measurement of thickness.....	33
Figure 3.4: Conductivity Vs Ag flakes weight% at 25°C.....	33
Figure 3.5: Change in resistance with temperature	35
Figure 3.6: Schematic drawing for the uniaxial stretching and releasing cycle and corresponding pictures of our experimental setup	36
Figure 3.7: (a) Change in resistance of the stretchable interconnect film during four stretch-release cycles. (b) Results in (a) are replotted in relative resistance versus strain curves to examine cycle to cycle variations.....	37
Figure 3.8: Relative resistance values with respect to strain up to the eventual failure at ~500%.....	38
Figure 3.9: Adhesion test using different methods.....	40
Figure 4.1: Schematics of elastic ink fabrication and the printing of stretchable traces onto elastomeric substrate for stretchable antenna fabrication.....	41
Figure 4.2: Antennas dimension (a) On-body type loop antenna (b) Patch and Bow-tie antenna. [Dimensions provided by H.A Damis and H. Saghlatoon, Device fabrication is done by Amit Kumar].....	42
Figure 4.3: Simulation model of the on-body antenna & the arm. Reproduced with permission from [59].....	43

Figure 4.4: (b, e, h) Simulation and measurement results of the input reflection coefficient for different length of On-body loop, patch and bow-tie antenna. (c, f, i) normalized radiation patterns of simulation and measurements of On-body loop, patch and bow-tie antenna. [measurements done by H. Saghlatoon and M.M.H. Kalateh]47

Figure 4.5: Vector network analyzer.....48

Figure 4.6: Fabrication steps of stretchable heater.....50

Figure 4.7: Printed heater at 0% and 80% strain on VHB. [Fabricated by T.G. La, A. Kumar]..50

Figure 4.8: (a) Printed heater on PET substrate (b) Microscopic image of the printed heater (c) SEM image [Fabricated by T.G. La, A. Kumar].....51

Figure 4.9: a) Applied current in cyclic process b) Resistance value in response to the applied current (c) Effect of temperature on optical properties of PA hydrogel. [Fabricated by T.G. La and A. Kumar].....52

Chapter 1. Introduction

1.1 Introductory overview of the thesis¹

The development of flexible and stretchable electronics rely heavily on the performance of interconnects that can withstand high deformation while maintaining electrical conductivity [1]. The stretchable interconnect is a key component to fabricate sensors and antennas for wearable electronics. An important aspect for wearable healthcare electronics is the ability to accommodate mechanical strain and deformation correlated with body motion without deteriorating the performance of the electronics [2]. Interconnects are passive component in electronics and are easier to accommodate deformation compared to active components such as sensors or integrated circuits [3]. In fact, many system-level integration of stretchable electronics has been achieved by assembling macroscopic integrated circuit chips (mm to cm scale) that are encapsulated in stretchable substrate [4]. In this case, stretchable interconnects and antennas are the only two electrical components that are actually stretchable. The printed stretchable interconnect can be achieved in numerous ways. Firstly, stretchability can be achieved even when the conducting material is not intrinsically stretchable. For example, metal films can be deposited on pre-stretched elastomeric substrate to achieve accordion-like ‘wavy’ structures[5] . Making structural relief in the metal patterns also allows stretchability, as can be exemplified by serpentine- [4] fractal- [6],

¹ Section 1.1 has been taken from the paper “A Highly Deformable Conductive Ink for Printed Antennas and Interconnects: Silver/Fluoropolymer Composite Amalgamated by Triethanolamine” to be submitted to *Flexible and Printed Electronics*

mesh-[7] , and coil-shaped[8] interconnects. These examples are not printed electronics, but their concepts can be easily applied in printing to achieve stretchability. Secondly, intrinsically stretchable, resilient, and conductive material can be developed. Percolating networks of nanowires embedded in or deposited on elastomeric substrate can be one example [9]. Metal precursor may be printed with elastomeric host materials and then reduced as a post-treatment to achieve conductivity [10, 11] as shown in fig 1.1. However, the post-treatment often involves high curing temperature or corrosive chemical that may lead to the degradation of the host or the substrate materials.

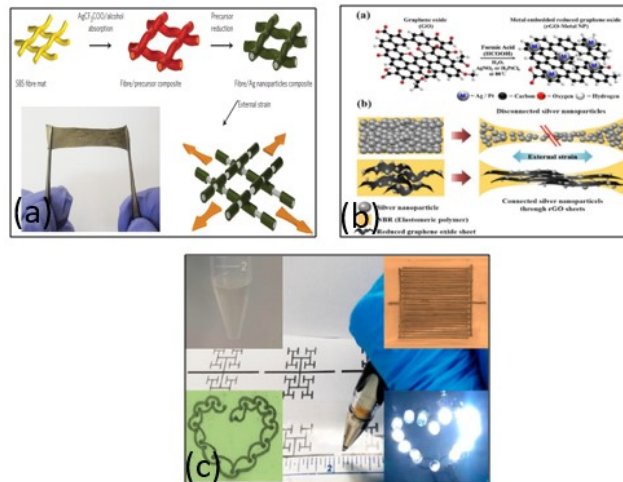


Figure 1.1 Reduction of metal ions. Reproduced with the permission from [9-11]

Thirdly, intrinsically plastic but non-resilient material can be filled and then encapsulated in elastomeric trough, like a microfluidic channel. A liquid-metal filled polydimethylsiloxane (PDMS) channel can be a good example[12] .

Enhancing printability to the conductive materials has been of research challenge. For example, Someya and co-workers introduced an imidazolium-based ionic liquid to achieve adequate viscosity of ink solution consisting of carbon nanotubes (CNT) and fluorinated rubber [13] as

shown in fig 1.2(a). This ink, however, has shown delamination issue between PDMS substrate and the interconnect layer. The group recently introduced a new formula that incorporates silver flakes, a fluorine rubber, and a surfactant to achieve enhanced adhesion on PDMS substrate (fig 1.2 (b))[14]. Baik and co-workers developed a printable silver and CNTs composite ink with polyvinylidene fluoride (PVDF) binder, but a rather high curing temperature of 160°C was necessary as shown in fig 1.2(c) [15]. Yang and co-workers developed a particle free conductive ink containing soluble Ag salt and adhesive rubber that allowed direct pen-writing as shown in fig 1.1(c). This ink could maintain good adhesion with polyethylene terephthalate (PET) and polyimide (PI), but multiple writing steps and chemical reduction post-treatment were necessary[16]. Pei and co-workers developed a water based silver nanowire ink with cellulose and

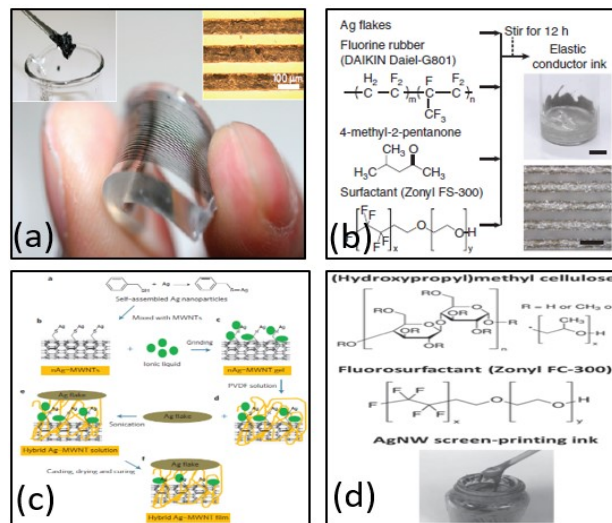


Figure 1.2: Composite based ink. Reproduced with the permission from [13-16]

fluoro-surfactant molecules [17] as shown in fig 1.1(d). Table 3 summarizes the key features of a few notable conductive inks for stretchable interconnects. An ideal ink of printable conducting material for stretchable interconnect will be to achieve all desirable traits, such as ideal viscosity

for printability, adhesion to various substrate, high deformability of conductive material, and low curing temperature.

Here, we developed a new formula to achieve a stretchable ink with high conductivity. We introduced triethanolamine (TEA), which has conventionally been used as a surfactant in cosmetic industries or a plasticizer in plastic manufacturing[18, 19], in our ink formulation of silver flakes and fluorine rubber. When fabricating the ink, TEA facilitated dissolution of the components in the co-solvent of methylisobutyketone (MIBK), resulted in a homogeneous solution. The ink could be easily printed and adhered well on various elastomeric substrates. After printing and drying of solvent, the composite exhibits high conductivity value of 8.49×10^4 S/m without any need for post-treatment. Moreover, TEA plasticized the composite so that the printed interconnects were freely deformable without losing the conductivity. The composite was not conductive by itself, but a combination of stretchable substrate and the composite's good adhesion allowed stretchable interconnect to be bended, twisted and stretched up to 100% without deteriorating its electrical and mechanical performances. We fabricated wireless local area network (WLAN) antennas with four different three different geometries: loop, patch, and bowtie. The performances of three different antenna geometries on human arm were simulated and measured for original geometry and uniaxially-strained conditions.

1.2 3D Printing Technology

In the recent years, several complex fabrication methods such as screen printing, photolithography, mask assisted printing has been employed for the fabrication of flexible and stretchable circuits. However, these methods are time- consuming and arduous to fabricate a complex pattern. Therefore, the direct printing of conductive inks/materials is a fast-facile process,

received a great attention due to its low material wastage, simplicity and flexibility which can be used for the fabrication of various devices such as wearable displays, flexible batteries and stretchable antennas. Therefore, the usage of 3D printer is an ideal choice, a versatile material conservation fabrication technique. It is an additive process where laying down of successive layers (horizontally or vertically) leads to the formation of 3D/complex structure from a digital file, which allows the users to form the desired product within few hours after CAD design completion [20]. Here we reported a brief overview about different additive manufacturing techniques such as fused deposition modeling (FDM), stereo-lithography and inkjet printing. All these methods are different in manner of building layers and the types of materials used to operate them. The key success of additive manufacturing depends on the proper optimization of the parameters while printing onto the substrates.

1.2.1 Fused Deposition Modeling (FDM)

It is a famous 3D additive manufacturing and extrusion technique used for modeling, prototyping and manufacturing [21]. In short, the filament is fed through the extruder and melted in the head before printing the final pattern as shown in fig 1.3. There are different optimized temperatures for all types of filaments. In case of better adhesion of the printed design into the bed, the base/bed temperature needed to be maintained around 65-80°C while printing.

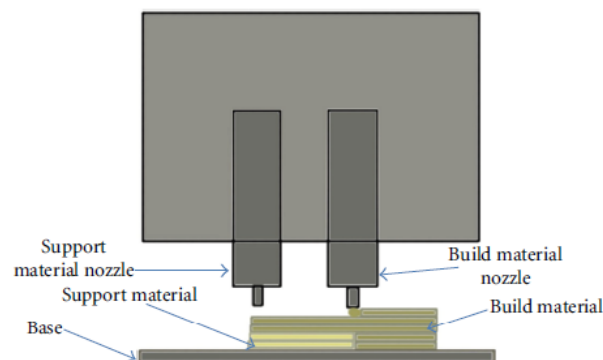


Figure 1.3: Fused Deposition Modeling. Reproduced with the permission from [22].

There are several advantages using FDM such as reduction in materials wastage, high throughput and easy to handle.

Notes for FDM Printer Operation: Fused deposition modeling (FDM) is the process of additive manufacturing technologies for numerous engineering applications. In this technique, a thermoplastic polymer feeds into the head of the printer, where it gets melted and extruded through the nozzle. The nozzle diameter varies from printer to printer. For the operation, it also needs a CAD file (created by modeling program) which can point the instruction to the printer. The .stl file is being created by using the CAD modeling program, followed by slicer tool. The slicer helps in converting the specific model into a series of thin layers and produces a G-code file containing instructions to a particular 3D printer. They are also known as FDM (fused deposition modeling) printers as shown in fig 1.4. The G code is then imported to the 3D printing clients such as Repetier - host, Replicator G for the final products. The materials which can be printed using such techniques are polycarbonate (PC), acrylonitrile butadiene styrene (ABS), PC-ABS blends, and thermoplastic polyurethane [23]. The major advantage of using FDM technique is that it is a cheaper method without any post treatment, polymer resin and UV exposure for producing the products. The quality of the printed structure through FDM depends on the precise selection of variables. For example, if the extruder temperature is too high corresponds to the filament melting temperature, then it can clog the nozzle orifice with the burnt filament.

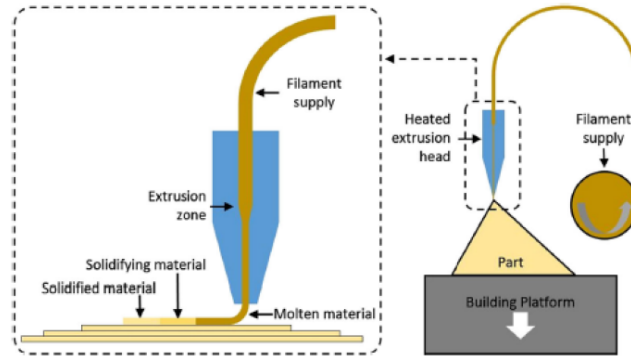


Figure 1.4: Extrusion AM process principle and schematic. Reproduced with permission[21]

FDM technique is a slow process and takes longer time while printing the complex structure. Dimensional measurement, base surface roughness and printed resolution are the most concerned parameters in FDM technique. The most important is the process control algorithm which controls the feed rate of the filament. So, the user has no control in additive manufacturing technique [23]. The printed part resolution and dimensional accuracy depends on the design parameters as well as the filament feedstock properties. Dimensional accuracy refers to fidelity of part geometry to the computer design [23].

1.2.2 Stereo-lithography

Stereo-lithography (STIL), the first technique which was widely used for rapid prototyping where the liquid polymer gets hardened by UV light exposure, developed by 3D Systems Inc as shown in Fig 1.5. It starts with CAD modeling tool and .stl extension file has been added to slicer tool which can cut the samples in slices and generate G- Code for the same [22] . There is also a need of the platform to anchor the piece and structures. Then, a highly-focused UV laser beam is applied above the liquid surface to produce the desired pattern by selectively curing the UV-sensitive liquid polymer gel in layer-by-layer manner. The platform gets lowered down after each layer completion. After printing all layers, excess resin get removed. The basic principle of such process

is the photo-polymerization, where a monomer or polymer can be converted to solidified object under UV exposure. This process is known as ultraviolet curing. If it is done for a longer time, the parts get dangle due to non-fusion of the bottom layer [22]. Stereo-lithography (SL) also give the options of using different materials while building a single piece, that is known as multiple material stereo-lithography. To print with different materials, there should be proper drainage system and replacement of new material at the same time.

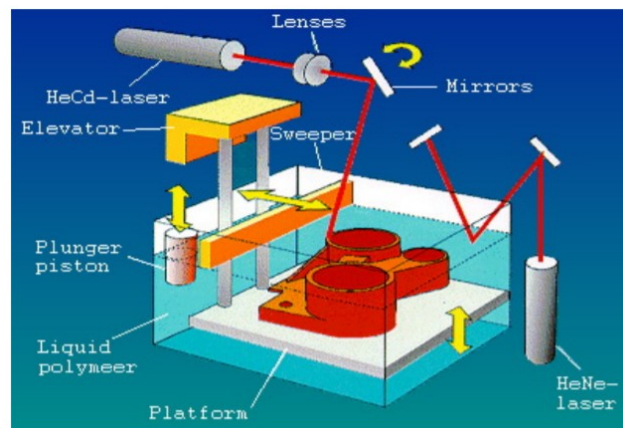


Figure 1.5: Schematic of stereolithography process. Reproduced with permission from [24]

1.2.3 Ink Jet Printing

Ink jet printing is a computer based digital printing by propelling the inks on the substrate. It works on two modes of operation: (a) DOD (Drop on Demand) mode and (b) continuous mode. In continuous mode, the ink is ejected from the nozzle in the form of jet breaks into small periodic parts due to the surface tension driven force whereas, in DOD mode, drop ejection takes place with the help of acoustic pulse and show small droplet size with better placement accuracy as shown in fig 1.6. Among these modes, DOD technique is highly preferred.

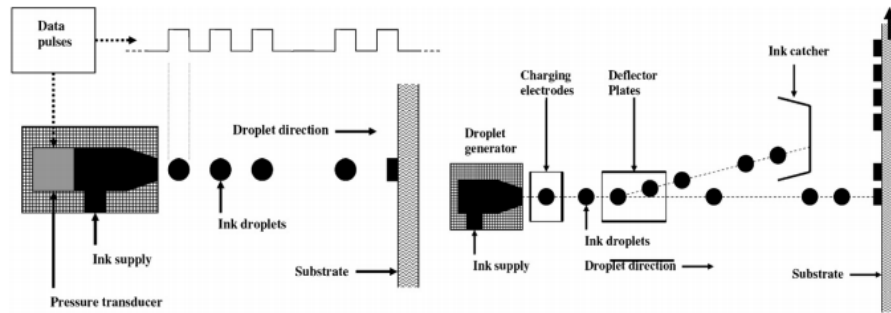


Figure 1.6: Schematic of Continuous mode- Inkjet printing and DOD printing. Reproduced with permission from [25]

Here whenever a positive pressure pulse is applied to the fluid inks in the supply tube, then ejection of fluid takes place. The droplet (coming out of the nozzle) total energy goes into viscous flow, surface tension and kinetic energy [26]. Ink viscosity and surface tension are some of the most crucial parameters in designing the ink for a printer. Therefore, the viscosity must be in ideal range and surface tension needs to be higher which makes the ink to grip to the nozzle without dripping. So, the first droplet is the major concern for printing which clogs the nozzle by partly dried ink. When the droplet impacts the substrate, one of the primary challenge is the feature resolution, which is totally controlled by the volume of droplet size. Thereafter, drying mechanism also takes place through solvent evaporation and elimination of coffee ring effect (discussed in chapter 2 in detail). In our work, we have used nScript 3Dn inkjet printer which operates in a different manner as compared to techniques described above. The details of nScript 3Dn inkjet printer will be discussed in Chapter 2.3.

Chapter 2. Fabrication procedure of Ag elastic ink

The fabrication procedure of silver elastic ink consists of four components such as fluorine rubber, 4-methyl-2-pentanone (organic solvent), triethanolamine (TEA) and silver (Ag) flakes. Herein we reported a simple and novel method to fabricate printable, highly conductive silver elastic ink, where no harsh conditions are required.

2.1 Materials and method²

2.1.1 Materials: Fluorine rubber (DAI-EL 801) was purchased from Daikin industries ltd, Japan. 4-methyl-2-pentanone (or methylisobutylketone; MIBK) and Silver (Ag) flakes (10 μ m, \geq 99.9% metal traces) and Triethanolamine (TEA) (\geq 99.0%) were purchased from Sigma Aldrich. A double sided clear transparent acrylic elastomer roll (VHB-4910) was purchased from 3M. All these reagents were used as-received without further purification.

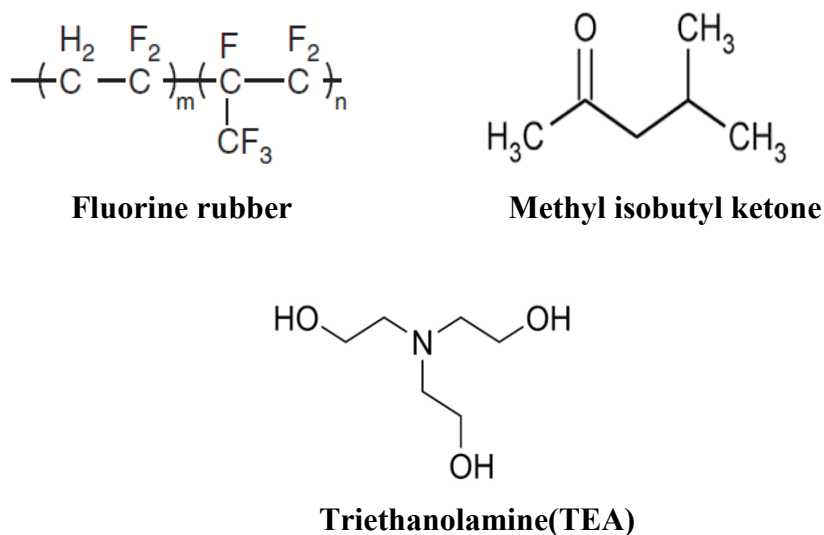


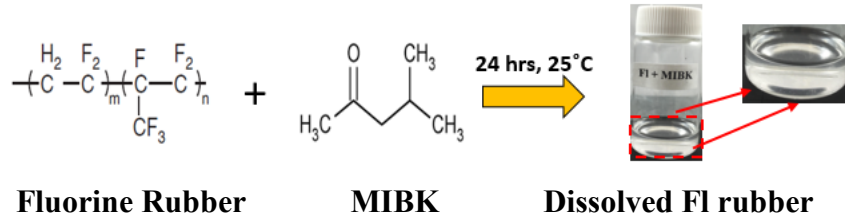
Figure 2.1: Chemical structure of the ink components

² Section 2.1 has been taken from the paper "A Highly Deformable Conductive Ink for Printed Antennas and Interconnects: Silver/Fluoropolymer Composite Amalgamated by Triethanolamine" to be submitted to *Flexible and Printed Electronics*

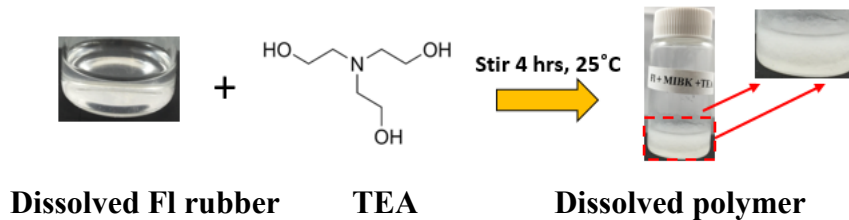
Fluorine (F1) rubber: DAI-EL G-801 is a fluoro-elastomer comprising copolymer of vinylidene fluoride/ hexafluoropropylene. It is translucent/light yellow in color with 66 weight% fluorine content and can be easily dissolved in low molecular ketones and esters. This material has excellent mechanical properties and chemical resistance. In terms of mechanical properties, it can be extended up to 440% strain of its original length. The above-mentioned ketone solvent was excellent in dissolving the fluorine elastomers, also volatilize easily due to high vapor pressure at room temperature, which is excellent for ink drying.

2.1.2 Preparation of highly conductive elastic ink: The mixing ratio of the four components is a vital parameter which is responsible for both mechanical durability and electrical conductivity of the elastic ink. We identified the optimal weight ratio between the fluorine rubber: MIBK: TEA: the Ag flakes to be 1:2.3:1:X in order to achieve both stretchability and conductivity. The X values are 2.95, 2.40, 1.90 and 1.45 for 40 wt%, 35 wt%, 30 wt%, and 25 wt% Ag content, respectively. Here, the nomenclature of 'wt% Ag content' refers to the total weight of the solution including the solvent. Firstly, fluorine rubber dissolved in MIBK for 24 hours. Then, TEA is added as a dispersive agent and the mixture was stirred for 6-8 hours. Once the mixture becomes homogenous, silver flakes are added and the mixture was stirred for 4 hours to attain the silver elastic ink. All these procedures were carried out at the room temperature. The antennas (On-body loop, patch and bowtie) were patterned onto an elastomer substrate (VHB-4910) by using a 3D jet printer (nScript tabletop 3Dn printer). After printing, antennas pattern were dried at 100°C for 20 minutes to remove the excess solvent. When complete drying is needed, samples were placed in a vacuum oven for 24 hours at 120 °C (Symphony-VWR, Vacuubrand 2C). The schematic of the fabrication procedure is shown in figure 2.2.

Step 1: Dissolution of Fluorine rubber



Step 2: Addition of TEA



Step 3: Addition of Ag flakes

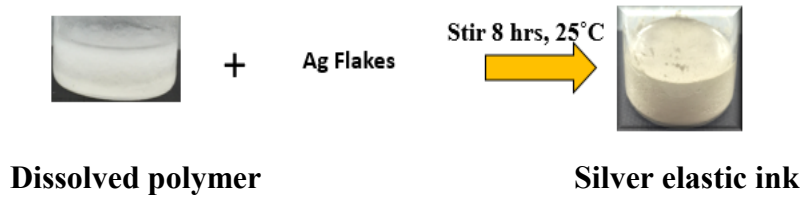


Figure 2.2: Steps for the preparation of 3D printable Ag elastic ink

2.1.3 Role of TEA in the elastic ink solution and in the stretchable traces

The elastic ink solution is composed of silver(Ag) flakes, fluorine rubber, an organic solvent (MIBK) and a dispersive agent (TEA). The role of TEA in our stretchable ink is two-fold: (1) compatibilizer between the components to ensure a uniform dispersion of Ag flakes (filler) in the matrix of fluorine rubber in ink solution state and (2) plasticizer for the PVDF polymer network, which bestows high stretchability in printed conductive trace state.

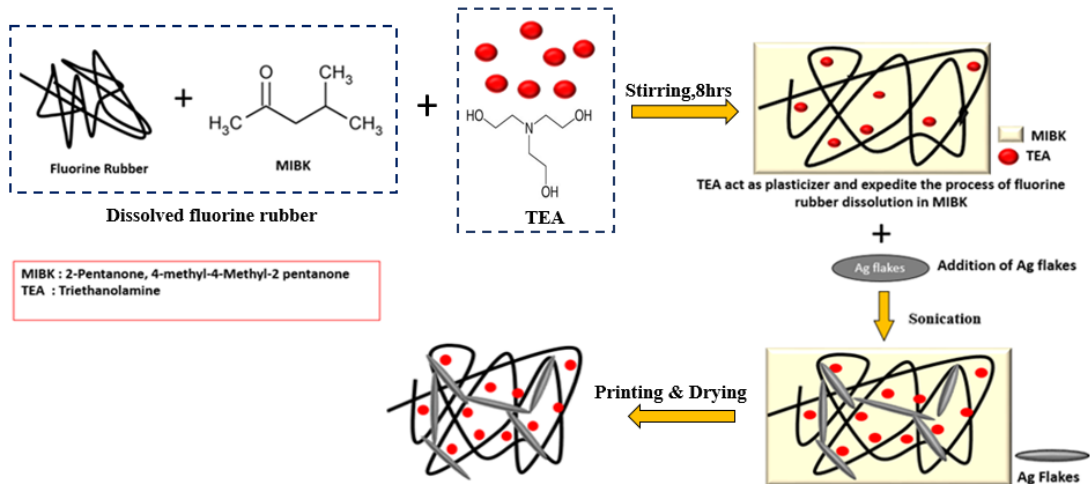


Figure 2.3: Schematic based on the role of TEA in fluoropolymer based elastic ink

TEA has long been used as an emulsifier to achieve complete wetting of water-soluble and oil-soluble ingredients in skin care and hair care products [27]. Due to the presence of 3 hydroxyl (-OH) groups and aliphatic chains on one molecule, TEA has also been used as a dispersing agent to disperse hydrophilic particles, such as titania [28] and hydroxyapatite [29, 30] in organic solvents for electrophoretic deposition (EPD) and as a surfactant for the surface stabilization of nanoparticles [31, 32]. In our case, TEA functions as a dispersing agent by establishing compatibility between Ag flakes and MIBK which drives a uniform distribution in solution state. After drying of solvent, TEA contributes the formation of percolating conductive network of Ag flakes inside the polymer matrix of PVDF. TEA also plays a role as a plasticizing agent. During the initial attempts to synthesize the stretchable ink solution, we found that the process of dissolution of fluorine rubber in MIBK was extremely time consuming. By the addition of TEA, the mixture dissolved homogeneously within a few minutes. This suggests that TEA diffuses into the fluoropolymer and quickly swell the network when in MIBK. In molecular sense, the compatibility may have been facilitated by the matching between the partial polarity of the hydroxyl groups in TEA and the polar C-F bonds in fluorine rubber. The swelling of the

fluoropolymer chains and their increased mobility can certainly facilitate the uniform dispersion of Ag flakes, whose surface is also compatibilized by TEA. The asymmetric molecular structure of TEA also aids in its high plasticizing ability [33], which gives high stretchability to the printed traces after drying out the solvent. Furthermore, very low vapor pressure of TEA (3.59×10^{-6} mm Hg at 25 °C) and high boiling point (335.4 °C) ensures that TEA molecules do not evaporate in low-temperature operating conditions, which is an excellent trait for a plasticizer [18, 34]. This point is supported by our TGA result as shown in Fig 3.2.

2.2 Selection of substrate

The selection of an appropriate substrate is an important initial step for printed flexible and stretchable electronics. In the substrate selection process, there is a need to determine the basic properties of the stretchable and flexible substrates as shown in the table 1. In addition, we found that our elastic ink strongly adheres to the VHB elastomer (VHB 4910 3M Company), which is useful for stretchable electronics application. Furthermore, it also has excellent mechanical properties, chemically stable as well as fast, clean, and simple to apply.



Figure 2.4: VHB 4910 3M Company

While selecting the substrates for stretchable electronic devices, it is also mandatory to know the value of some important parameters such as dielectric constant (ϵ), substrate thickness, and loss tangent ($\tan \delta$) of the substrates for the application purposes.

Table 1: Properties of various substrates

Substrates	Surface Energy (Dynes/cm)	Loss tangent	Dielectric constant	Deformability	Ref
VHB	38-39	0.03 at 1GHz- 5GHz*	3.20 at 1GHz-5GHz*	High	[70]
PDMS	23	0.01-0.05 at 1GHz - 5GHz 0.02 at 3GHz 0.05 at 3.45GHz 0.0134 at 2.4 GHz	2.67-3.0 at 1GHz – 5GHz 2.80 at 3 GHz 3.00 at 3.45GHz 2.7 at 2.4 GHz	High	[71] [35] [36]
Kapton Polyimide	40	0.002 at 2.45GHz	3.24-3.4 at 2.45GHz	Low	[71] [37] [38]
PET	42	0.01 at 2.45GHz	4.0 at 2.45GHz	Low	[71] [39]

* values experimentally measured in this study (with dielectric measurement probe by M.M.H. Kalateh and H. Saghlatoon in Prof. Mousavi's lab)

After measurements, value for $\tan \delta$ and ϵ values are found to be 0.03 and 3.20 with the substrate thickness of 1mm. The dielectric constant (ϵ) is a complex parameter. In equation,

$$\epsilon = \epsilon_0 \epsilon_r = \epsilon_0(\epsilon'_r - \epsilon''_r)$$

Where ϵ_0 (the permittivity of vacuum) = 8.854×10^{-12} F/m

In general, the dielectric property depends on the frequency, temperature, moisture content, homogeneity, and surface roughness. The ratio of the imaginary to real part called tangent loss.

$$\text{Loss tangent, } \tan \delta = \epsilon''_r / \epsilon'_r$$

The low dielectric constant value substrates helps in reducing the surface wave losses which are being tied to guided wave propagating and highly recommended for high frequency applications [40]. If the dielectric constant (ϵ) value is higher, waves concentrate more onto the substrate

because of the polarization of the electric field is stronger inside the substrate. Thus, it is superior to use a low dielectric constant (ϵ) substrate which increases the spatial waves in the surroundings and hence increase the impedance bandwidth of the antenna making it more efficient with high gain. Moisture content in the substrate affects the permittivity value which results in bandwidth change [40]. Therefore, usage of low dielectric constant (ϵ) substrate such as VHB, PDMS and PET are highly recommended which have additional features such as flexibility, re-configurable and capability to work at higher frequency because of the low dissipation factor (loss tangent). Loss tangent describe the inherent dissipation of electromagnetic energy in the dielectric material used for antenna fabrication because higher the value, more will be dissipation within the substrate resulting in lower radiation, hence, the efficiency decreases. Therefore, lower the loss tangent value, better would be the antenna performance.

Substrate thickness: As we mentioned above the thickness of dielectric substrate is also an important parameter for the designing of antenna. When the value of k is fixed, the substrate thickness may be chosen to maximize the bandwidth of the proposed antenna. But the substrate thickness is not the only parameter which can optimize the antenna efficiency.

Bandwidth $\sim 1 / Q$ (quality factor)

Therefore, thickness of the substrate is one of the factor influencing the bandwidth. If the height of antenna increases, Q factor decreases which will increase the bandwidth of the antenna by allowing a thicker substrate [40, 41]. Here, we have chosen acrylic VHB elastomer with thickness of 1mm for stretchable antenna and heater applications.

2.3 nScrypt 3Dn printer and its components

I used nScrypt 3Dn printer to print the elastic ink onto various elastomeric substrates. It consists

of two pumps: an nFD pump for 3D printing of polymeric filament (FDM printing) and a Smart Pump for jet printing of fluidic ink. In case of ink printing, smart pump consists of variable sizes tips in 12.5 μm - 175 μm range (as shown in fig 2.5). They can be controlled using digital input and can be programmed to accommodate a wide range of materials. In fact, the strongest feature of nScript 3Dn printer lies in its proprietary jet printing technology that enables printing of fluids with viscosity ranging from 1 cP to 1 million cP. Materials such as particles, flakes and tubes can be loaded and form low viscosity inks having nanoparticles to extremely high viscosity pastes, whereas flakes maintain good control, small features and fast prints. It is possible to print lines as narrow as 12.5 microns.



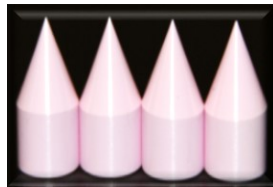
nScript 3Dn tabletop printer



Ink Smart Pump



nFD Pump



Nozzles



Ink printing

Figure 2.5: nScript 3Dn printer and its parts [69]

2.3.1 Printing Procedures: Before printing, it requires numerous calibration and actuation steps for the operation of smart pump. The conductive elastic ink printing onto the substrate can be done by using variety of approaches. First, the syringe filled with the conductive ink elastic is mounted onto the printed head along with positive pressure pipe; which is followed by the assembly of several other components such as valve rod, O-rings, and nozzle onto the smart pump. There are several other steps such as PCAD file conversion to path file, import path file, editing of path file, height test and teach origin before start printing. So, whenever a positive pressure is applied onto the mounted syringe on the print head, it starts feeding the materials into the valve body. To start micro-dispensing, valve will open and allow the material to flow smoothly through the nozzle orifice onto the polymer surface [42]. The valve rod moves to a closed position to stop ink dispensing which not only blocks the channel, but also maintains a negative pressure in the dispensing tip chamber. The valve rod which is responsible for ink flow move up and down with the motor support. The patented ceramic dispensing tip in our work reduces the pressure of outcoming material through the nozzle orifice. Such smart pumps can control the materials volume flow up to pico-liter level with higher speed printing and handle inks having high viscosities and loaded materials. The major advantage of 3Dn printer is low material wastage because there is fraction of milliliter dead volume in the entire pump [42].

2.3.2 Nozzle diameter: The nozzle diameter decides the resolution of direct printing. In our work, we patterned with the nozzle, made up of ceramic, having diameter of 125-175 μm for printing. As we know, patterning of thin line is quite challenging which highly depends on nozzle diameter. If the particle diameter is just 5% larger than the nozzle, it will clog the nozzle [43]. Smaller particles

also can cause jamming at the nozzle, which results in a catastrophic clogging. We also observed the clogging issues with smaller nozzle diameter(50um) by silver flakes whose size was around 10um. However, high resolution could be achieved by making the smaller nozzles whose manufacturing is quite challenging because once the clogging issue starts occurring, leads to the non-repeatability of the nozzle and increases its manufacturing cost [43]. Therefore, in our work, we preferred to work with larger diameter nozzles due to the large particle sizes.

2.4. Drop Impact and Spreading Behavior

When a liquid drop falls onto the substrate, then the phase change will take place which will help in transforming the liquid drop into a solid. Such phase change comes up with desired product, otherwise additional step sintering is required. The droplet impact on hard surface can be controlled by multiple physical factors such as inertial, capillary and gravitational forces. The important dimensionless terms to determine the drop behaviors are the Reynolds, Weber, and Ohnesorge numbers along with the bond number (Bd), where gravitational forces [44].

The droplet impact can be divided into three stages: contact, spreading and recoil. When a droplet contacted with the substrate, a thin circular film formation takes place around it. The radius of the circular film must be greater than that of in-flight droplet radius because of the kinetic energy dissipation of the droplet. When the drop starts spreading, liquid will make radially outward flow and there would be mass accumulation obtained at the periphery to form a liquid ring which is called coffee ring effect. Some part of the kinetic energy is dissipated because of the viscous flow within the thin film. Recoiling of film occurs when it reaches to the maximum value. Finally, the fluid comes to steady state after a number of inertial oscillations, which gets further dampened by viscous dissipation (shown in fig 2.6). In all cases mentioned above, the solidification will take

place after the deposition of ink, and the printed pattern must have some stability in the liquid state prior to solidification [45].

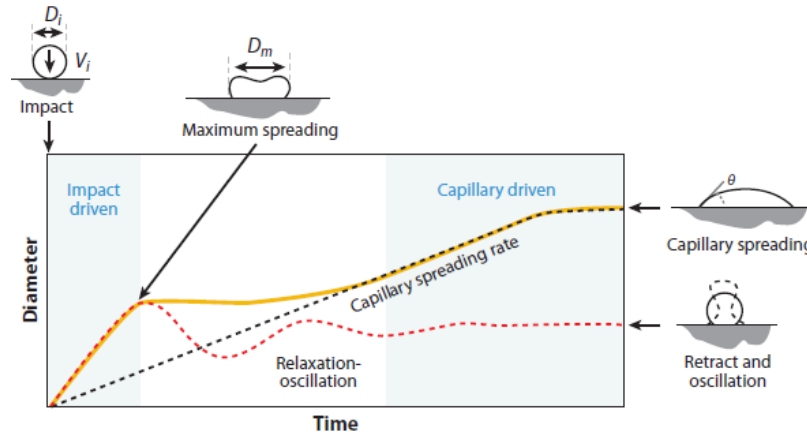


Fig 2.6: Schematic illustration of the sequence of events that occurs after droplet impact on a substrate. Reproduced with permission from [44].

The contact angle also plays an important part in controlling the resultant shape of the printed pattern. As the drop falls on the substrate then contact diameter (d_{con}) increases, the contact angle would certainly decrease. When the drop spreads after impact, the contact angle would be advancing angle rather than equilibrium angle [44, 46]. However, while forming the pattern onto the substrate, drop interaction may take place with the neighbouring drops. Such interactions can cause flow reversal and then receding angle plays a vital role. Receding angle play a major role in drop solidification during solvent evaporation. Decreasing the receding angle means decreases the drop volume and surface area. However, droplet drying occurs due to the contact line pinning from solute deposition which help in increasing solvent evaporation rate from the edge and migrate the solute particles towards the side which give rise to a phenomenon called coffee stain effect [44, 46]. The contact diameter of spreaded drop (d_{con}) is obtained by its volume and equilibrium contact angle (Θ_{eq}). To determine the size of the droplet, bond number (Bd) should have least value which permits the shape of spreaded drop can be taken as a sphere shape [47].

$$d_{\text{con}} = d_o \sqrt[3]{\frac{8}{\frac{\tan\Theta_{\text{eq}}}{2} \left(3 + \frac{\tan^2\Theta_{\text{eq}}}{2}\right)}}$$

The resolution of the inkjet printing is determined by the droplet contact diameter onto the surface; a linear function of the drop flight diameter.

2.4.1 Rheology Control

When droplet impact and spreading takes place, ink rheology is of great importance, which is affected by numerous parameters such as concentration of polymer additives, solvent composition, surfactants and dispersion quality. In general, most of the inks have Newtonian behavior, with constant viscosity over a wider range but non-Newtonian inks are also available [48, 49]. It was observed that sedimentation of large particles will occur, if the particles are larger in size. Therefore, large efforts are being made to obtain particles as small as possible in the ink manufacturing for printing. To prevent the particle sedimentation and non-Newtonian behavior, controlling viscosity is the only available option left for the ink designer. In general, it has been found that the ink has high viscosity during storage and low viscosity during jetting conditions [48, 49]. Due to the different shear rates during storage and jetting can lead it to the formation of non-Newtonian ink. Such type of behavior would certainly affect the ink properties such as ink flow through the printing system, droplet ejection and satellite formation.

2.4.2 Droplets phase behavior and Stability

When the ink droplets interaction takes place, then there would be possibility of two phase transfer processes. Firstly, kinetic energy dissipation will help in spreading droplet onto the substrate. The

spreading of the droplet onto the surface totally depends on the surface wettability and viscosity, and wait until it reaches the equilibrium shape with the balanced forces. Therefore, the stability of the pattern is required before solidification takes place at the liquid state. There could be number of reasons for the occurrence of phase change such as solvent evaporation, cooling through a transition temperature, chemical reaction and polymer precursor gelation [50]. In the initial phase of droplet phase change, the characteristics time scale is given by the relation $t = R_o / U_o$, where R_o is the initial droplet radius and U_o is impact velocity with which droplet fall onto the substrate. In general, value of characteristics time scale is lesser than 1ms in inkjet printing [51].

After the initial phase, it is being followed by the drying phase, where the solvent evaporation takes place and formed a solid residual layer remains after the solvent evaporation. The timescale of the drying process totally depends on the ambient temperature, droplet radius and humidity level. In general, it is found in the order of few seconds for inkjet printing. It displayed that the two phases, spreading and drying takes place in a distinct way [51]. So, the processes taking place during the drying phase showing interesting behavior and are of crucial importance. In most of the cases, such processes are enough but sometimes there is a need of sintering process too. Therefore, it is crucially importance to understand the phenomenon involved between the printed pattern and substrate before solidification occurs.

The below available equations are derived for droplet generation and concentration of solute while drying process occurs which is only valid when the droplet size is in micrometer range. The initial point of the droplet derivation is the Navier-stokes equation [51]. It has been assumed that liquid has incompressible nature of the droplet, then the Navier-stokes equation can be written as

$$\frac{\rho \partial u}{\partial t} + \rho u \cdot \nabla u = -\nabla p + \eta \nabla^2 u - g e_z$$

And the continuity equation is given by

$$\nabla \cdot \mathbf{u} = 0$$

Where \mathbf{u} is the fluid velocity, p is the pressure; ρ and η are mass density and dynamic viscosity of the fluid, g is the gravity acceleration which points in the negative direction.

The order of magnitude of numerous distinct terms in above equation can be determined by the insertion of characteristics value for horizontal size, R and vertical size of the liquid droplet, H . Such values corresponds to the radius and height of the droplet when the initial spreading phase takes place [51]. When the vertical velocity component of the liquid equals the evaporation velocity which is averaged over the droplet surface, $v_{e,av}$ the calculated value for the horizontal velocity is given by

$$V = v_{e,av} \frac{R}{H}$$

If there is comparison between the droplet radius and its height, then horizontal velocity is large as compared with vertical velocity. In further part, split the velocity in its horizontal component u_{\parallel} and vertical component which is given by $\mathbf{u} = u_{\parallel} \mathbf{e}_{\parallel} + w \mathbf{e}_z$ [51]. Therefore, the horizontal and vertical component of the Navier - stokes equation can be written as

$$We \left(\partial \frac{u_{\parallel}^*}{\partial t^*} + \mathbf{u}^* \cdot \nabla u_{\parallel}^* \right) = - \frac{R}{R_C} \nabla^* P^* + Ca \left(\frac{\partial^2 u_{\parallel}^*}{\partial z^{*2}} + \frac{H^2}{R^2} \nabla_{\parallel}^2 u_{\parallel}^* \right)$$

and also

$$We \left(\partial \frac{w^*}{\partial t^*} + \mathbf{u}^* \cdot \nabla w^* \right) = - \frac{R^3}{R_C H^2} \frac{\partial p^*}{\partial z^*} + Ca \left(\frac{\partial^2 w^*}{\partial z^{*2}} + \frac{H^2}{R^2} \nabla_{\parallel}^2 w^* \right) - Bd$$

Here asterisks used for scaled variables and ∇_{\parallel} represent the horizontal component of the gradient operator. Ca is the capillary number which is given by

$$Ca = \frac{\eta V}{\sigma} \frac{R^2}{H^2}$$

We is the weber number and given by

$$We = \frac{\rho V^2 R}{\sigma}$$

And Bd is the bond number which is given by

$$Bd = \frac{\rho g R^2}{\sigma}$$

Finally, R_c is the radius of curvature which gives σ / R_c value for pressure [51].

Printable Fluids/ Droplet generation

The droplet generation in the inkjet printing is a complex process. The characteristics of the droplets can be determined by the number of dimensionless constants such as weber number, Reynolds number, Bond number and Ohnesorge number [44].

$$\text{Reynolds number, } Re = \frac{V\rho R}{\eta}$$

Similarly, Ohnesorge number is a dimensionless number and defined as the ratio of viscous force to inertial and surface tension force. This ohnesorge number is used for determining the behavior of the drop impacting onto the substrate. The equation for Oh number is given below

$$\text{Ohnesorge number, } Oh = \frac{\text{Viscous forces}}{\sqrt{\text{inertia} \cdot \text{surface tension}}} = \frac{\sqrt{We}}{Re} \sim \frac{\eta}{\sqrt{\sigma\rho R}}$$

Where W_e and R_e are the Weber and Reynolds numbers for the flow, η is viscosity of the liquid σ is surface tension, ρ is density of the ink and d is orifice diameter.

Here Oh is not dependent on the velocity of the fluid. The value of Oh must lie between 0.1-1 in order to avoid the formation of large number of small drops called satellite formation. It also helps in disturbing the fluid instability for the satellite drop formation. Finally concluded that while printing, the intervals of the energy number E_n (ratio of kinetic and surface energy) and the inverse

Ohnesorge - number Z^{-1} (depending upon printing system) for inks must be between 0-1 and 1-10 respectively, to avoid satellite drop on the substrate surface.

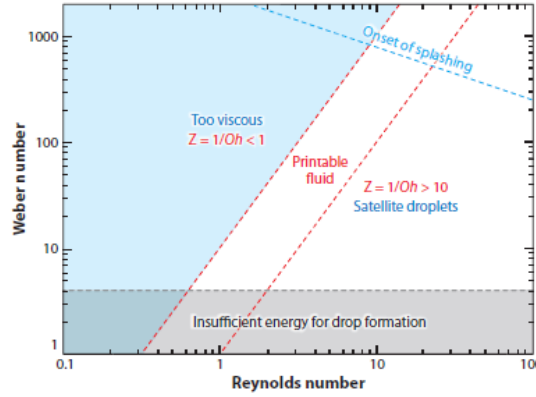


Figure 2.7: Fluid regime properties in DOD. Reproduced with the permission from [44]

Reis et.al shows that value of $10 > (Z=1/Oh) > 1$ range, for stable drop formation as shown in fig 2.7. At the lower values of Z , viscous dissipation stops drop ejection through the nozzle, whereas at high values of Z , the first droplet guided with numerous satellite droplets formation [44, 52]. For the droplet generation, there are some other limiting factors available at the liquid/air interface. The ejection of droplets through the nozzle orifice needs sufficient energy to overcome the barrier [53]. The minimum velocity for droplet ejection through the nozzle orifice is given by

$$V_{\min} = \left(\frac{4\sigma}{\rho d_n}\right)^{1/2}$$

Above equation in terms of weber number, the minimum value for printing is given by

$$W = V_{\min} \left(\frac{\rho d_n}{\sigma}\right)^{1/2}, \text{ Where } d_n \text{ is nozzle diameter } \sigma, \rho \text{ are the surface}$$

tension and density.

2.4.3 Ink Drying

The deposition of particle morphologies can be controlled by varying the components concentration. The ink drying phenomenon totally depends upon the volatility of the solvent. It

undergoes through three regimes: constant diameter, constant contact angle, and both before the final chaotic regime [50]. In the case of constant diameter, there is a linear evaporation of the droplet from the overall surface with decreasing the contact angle and height till the receding angle is reached. In other case, contact angle remains constant or at a fixed value, while the diameter gets shrinks. Finally, both the diameter and contact angle shrinks until the evaporation process gets completed. In general, it was observed that droplet with lower value of the initial contact angle has high evaporation rates and occurrence of linear mass loss during the drying process [50, 51].

Mechanism: When the droplet drying occurs, it utilizes the evaporation-induced flow which is the combination of radial and Marangoni flow. The radial flow is also called evaporation induced radial flow which made solutes particles to move to outer periphery of the droplet due to the higher evaporation rate at the droplet edge. In Marangoni flow, surface gradient plays a major role between the periphery and droplet interior from the region of low to high surface tension [50, 54]

If the minor component in the mixture has higher boiling point with low surface tension than the major solvent, which leads to droplet recirculation in the counter direction and Marangoni flow occurs. When the minor component has lower boiling point with high surface tension then the Marangoni flow helps in enhancing the radial flow (shown in fig 2.8). So, the evaporation-induced radial flow totally depends on the solvent mixture composition. It is almost similar to coffee ring effect [54, 55]. Therefore, they used the solvent mixtures to balance the Marangoni and radial flow. Here controlling the morphology of the drying droplet is a major concern. To increase the homogeneity of printed films, mixtures of low-boiling good solvents and high-boiling solvent inks under consideration were used.

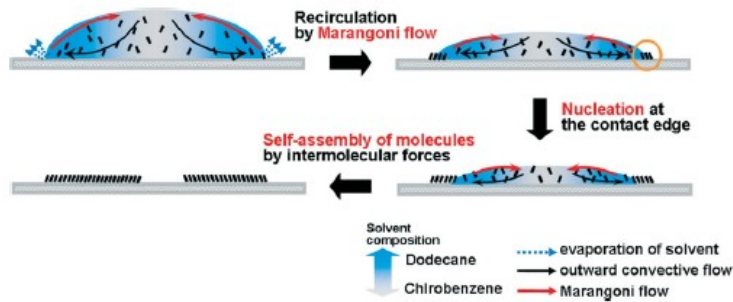


Figure 2.8: Self-organization of solute during drop drying using marangoni flow.

Reproduced with the permission from [54]

The usage of a binary mixture of solvents in polymer solution can remove the formation of ring stains, when one of the solvent in the mixture has a much higher boiling point than other. Due to solvent evaporation and Marangoni flow, uniform thickness of the film can be obtained.

Reduction of coffee stain effect

The coffee stain effect can be reduced by using the heated substrate because the material transfer to the contact line is minimized but the evaporation rate got highly increased at the deposited features [50]. The other way to reduce it is by increasing the contact angle of the printing pattern or increase the solution concentration.

Chapter 3. Characterization of ink properties

After the development of elastic ink, measurement of several ink characteristics has been carried out. Thus, it has been divided into two sections (i) physicochemical properties of the ink (ii) mechanical durability of the ink. The physicochemical properties include viscosity measurements, thermal degradation of ink components, conductivity variation and temperature effect on resistance where as the mechanical properties includes conductivity variation with stretchability as well as multiple stretch-release cycle. All these measurements were done using different tools as described in the section below.

3.1 Characterization Techniques

The morphology of Ag flakes was characterized by scanning electron microscopy (Zeiss EVO M10 SEM - imaging). All samples drying were carried out in a vacuum oven at 120 °C (Symphony-VWR, Vacuubrand 2C). Further, sample loading/unloading tests were performed on Instron tensile tester (Instron 5649). Thermo-gravimetric analysis (TGA) was performed by using TGA-Q550 tool. Thermo-camera (Seek Therma CompactXR Smartphone Thermal Camera) was also used to see the film surface temperature. The viscosity measurements were done on a viscometer (Anton-Paar) at room temperature. The film thickness was measured by using profilometer and resistance was measured using Keithley 2400 source meter (Keithley instruments).

3.2 Physicochemical properties of the ink³

3.2.1 Viscosity measurement

Ink viscosity is a vital parameter which has direct influence on printability resolution. In case of solution based ink, there should be perfect loading of the solute particles in the ink and dried in a controlled manner at the substrate–ink interface to avoid the volumetric cracks. They are totally dependent on the ink viscosity and solvent volatility, which can provide the good resolution print once the rheological properties of ink are known along with the surrounding environmental condition. In the case of suspension-based inks, which consists of colloidal suspensions and particles (micro and nano range), grant the ink manufacturer to exceed solubility limits significantly by enhancing the weight loading and producing more durable films. However, such suspensions may have fixed shelf-life beyond which can lead to the formation of aggregation, precipitation and instability of the ink.

The operation of 3Dn jet printer completely depends on the viscosity of the ink flowing through the nozzle orifice which can be affected by the rapid solvent loss. It is mandatory to attain the proper ink viscosity within the approachable limits. Here number of viscosity tests at set intervals were carried out to verify the ink stability and printer ink requirements. The viscosity of the particle suspension is non-Newtonian, which implies that it is a function of shear rate. In case of inkjet printing, the printers have a limit on two important parameters, namely ink viscosity and the shear rate (or the frequency) at which the ink comes out of the nozzle. The maximum allowed viscosity of the ink is 0.02 Pa-s and the shear rates fall in the range of 10^3 - 10^4 s⁻¹[56]. In this case, the

³ Section 3.2 has been taken from the paper “A Highly Deformable Conductive Ink for Printed Antennas and Interconnects: Silver/Fluoropolymer Composite Amalgamated by Triethanolamine” to be submitted to *Flexible and Printed Electronics*

viscosity of elastic ink measured was between 0.3 Pa-s and 1.1 Pa-s (at 25°C) at different concentration of silver flakes (25-40 wt. % respectively) by using viscometer at shear rates from 60 to 100 s⁻¹. The variation of viscosity with shear rate is shown in figure 3.1.

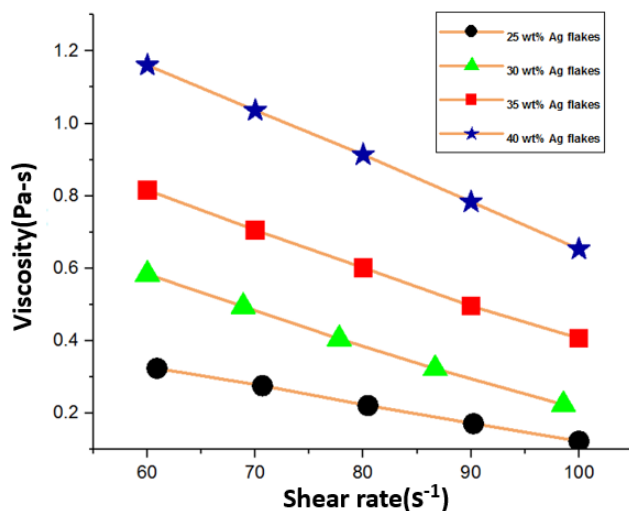


Figure 3.1: Viscosity variation with shear rate

As seen from the figure, viscosity shows a decreasing trend with shear rate at all concentrations taken, which reinstates the fact that the elastic ink shows shear thinning behaviour. The viscometer has a maximum shear rate limitation of 1550 s⁻¹ and this falls in the lower end of the range of shear rates used in inkjet printing. On extrapolation, the data indicates that the viscosity of all four concentrations of Ag flakes would fall below 0.02 Pa-s at shear rates above 1000 s⁻¹ and it would be difficult for the viscometer to produce accurate values at such low viscosities which requires high shear rates. Thus, we can conclusively state that this ink conforms to standards of inkjet printing and can be used without any hassle. Therefore, it is concluded that ink viscosity decreases with increase in shear rate as well as with decrease in Ag flakes concentration from 40 to 25 wt. % by keeping concentration of other components as constant.

3.2.2 Thermal stability of elastic ink and its components

Thermal gravimetric analysis (TGA): It is a technique which helps in measuring the mass/weight loss of the material as a function of temperature while sample is placed in a controlled atmosphere. An alternate definition to remember, which measures a sample's weight when it is heated or cooled in a furnace. It is having a pan which is being supported by precise balance. The monitoring of sample mass is done during the experiment. It can help in quantifying number of information such as water loss, solvent loss, plasticizer loss, oxidation, decomposition, weight % filler and weight % ash. The typical size ranges from 5-20mg or little more. Instead of one large chunk, small pieces of respective sample are preferable in TGA. The explosion of large surface area is better to the sample purge.

Thermal degradation of the printed trace (fluorine rubber + TEA + Ag flakes; 0.72) is an important measure to assess maximum processing temperature after printing. We studied the property of the printed trace and three control samples using thermal gravimetric analyzer (TGA; TA Instrument Q500) in N₂ gas at a heating rate of 10 °C/min from 30 °C to 700 °C (Fig. 3.2). In all the samples, the solvent (MIBK) was completely removed by vacuum oven drying at 120 °C for 24 hours. The three control samples, TEA, fluorine rubber, and fluorine rubber + TEA (at the mixing ratio of 1:1), were selected to study the effect of each component and the influence of mixing. Fluorine rubber seemed stable up to ~400 °C. TEA appeared to be volatile at temperatures as low as ~170 °C. The reported boiling point of TEA is 335.4 °C and is non-volatile at room temperature (3.59×10^{-6} mm Hg), but the volatility rapidly increases at higher temperatures (for example, 10 mm Hg at 205 °C) [57]. Mixing with fluorine rubber significantly suppressed TEA's volatility; even stronger effect was observed when mixed with Ag flakes.

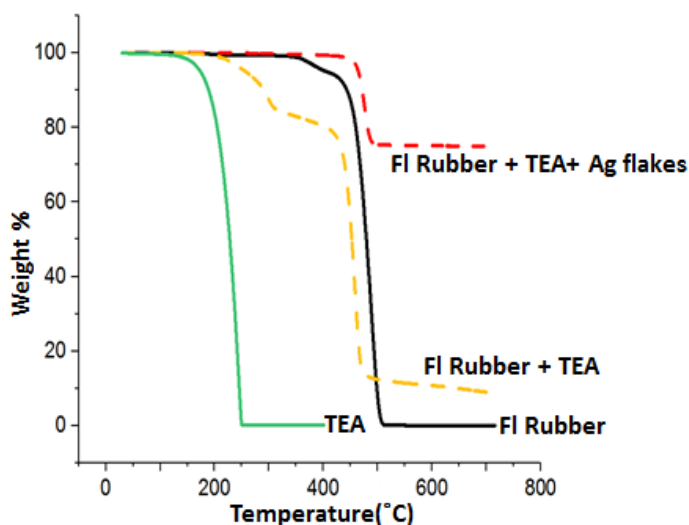


Figure 3.2: TGA of conductive ink and its components

Here, only 25% of weight loss was observed for the printed trace after the TGA cycle up to 700 °C. If more than 90% of TEA and fluorine rubber are to be volatilized at 700 °C, as shown in the result of the fluorine rubber + TEA, the projected weight loss is ~60% as shown in fig 3.2. Interestingly, we observed the formation of black char residue in the printed trace sample after the TGA cycle, which suggest that there was some silver-mediated chemical reaction of fluorine polymer and/or of TEA. Further chemical analysis is required to elucidate this phenomenon.

3.2.3. Conductivity variation with silver content wt.%

Here we prepared conductive elastic ink with different weight% in a controlled manner at room temperature. For the conductivity measurement, elastic ink is directly printed onto the elastomeric substrate using 3Dn printer, after drying at 80°C for 30 min, then it is connected to two copper electrodes along with the multimeter. In each of the case, film thickness and surface smoothness was measured using profilometer. It is arduous to control the thickness of the film while printing and average film thickness was found to be 20-70µm for all the different wt.% samples.

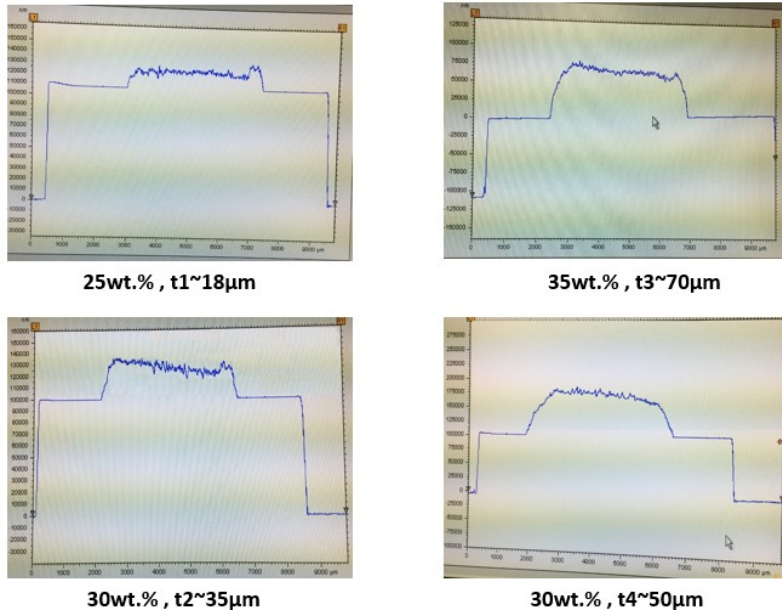


Figure 3.3: Measurement of thickness

Figure 3.3 shows the variation of conductivity of the printed trace with respect to the content of Ag flakes. The electrical conductivity increased monotonically with increasing Ag flake loading between 25wt% and 40wt% of the weight of the total ink solution including the solvent. To calculate the conductivity of the printed film,

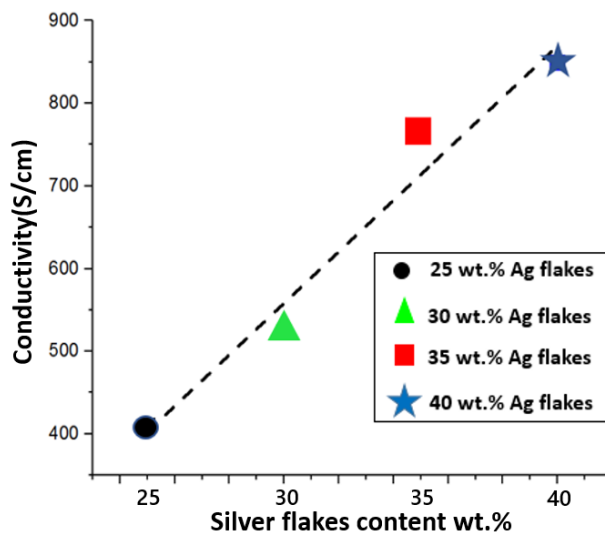
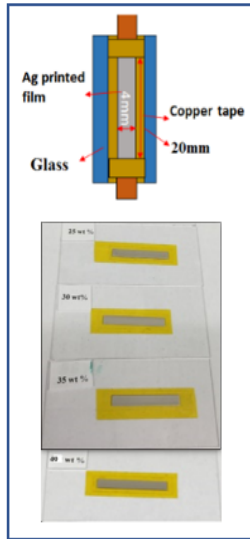


Figure 3.4: Conductivity Vs Ag flakes weight% at 25°C

Table 2: Conductivity measurements with Silver content wt.%



S.no.	Ag content (wt%)	Thickness(um)	Dimension (mm)	Conductivity (S/m)
1	25	18	L=20 ,W=3	4.1 * 10 ⁴
2	30	35	L=20 ,W=4.2	5.23* 10 ⁴
3	35	70	L=22 ,W= 5	7.61*10 ⁴
4	40	50	L=14 ,W=4.2	8.49*10 ⁴

The conductivity mechanism is explained by percolation theory; as per which, a continuous mechanical network is formed between the silver flakes of elastic ink, which act like bridges for the conduction of electrons. Here, the maximum conductivity value of 8.49*10⁴ S/m was achieved in the 40 wt.% Ag loading and minimum value of 4.1*10⁴ S/m in the 25 wt.% Ag (as shown in table 2), which is calculated by using the following equation: $\sigma = \frac{1}{\rho} = \frac{L}{RWt}$ where σ , L, R, W, t are the conductivity, length, resistance, width and thickness of the printed film.

3.2.4 Temperature effect on the resistance

Once the Ag elastic ink (with 30 wt.% and 35 wt.% silver flakes) was printed onto elastomeric substrate, it was cured in a vacuum oven at 120°C for 24 hours to remove the excess solvent. After the complete removal of solvent, change in resistance was measured with varying temperature from 30°C to 110°C by fabricating two copper electrodes connecting the printed lines to a

multimeter. During measurements, the surface temperature of the printed film was monitored continuously by using thermal camera. In our experiments, each reading was recorded after the temperature gets stabilized at an interval of 10 minutes.

Figure 3.4 shows the temperature dependences of the change in resistance values with respect to each sample's 25 °C values. When temperature increases from 25 °C to 110 °C, both samples exhibit positive temperature coefficients of resistance due to thermal vibration of atoms within the printed film, hence making the electrons flowing through the film more likely to collide with one of the atoms.

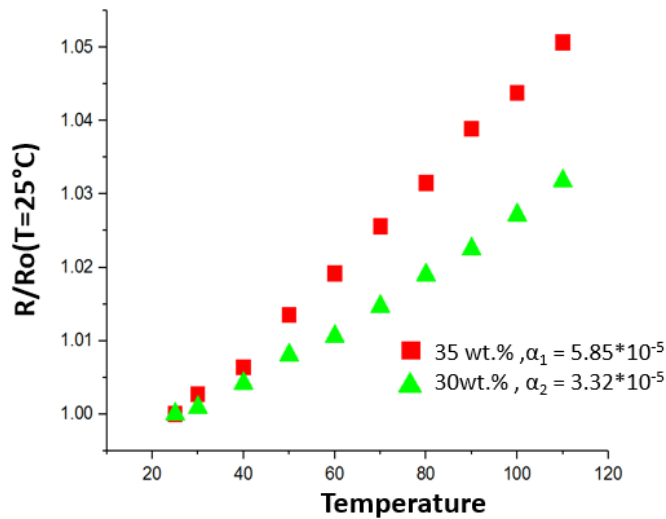


Figure 3.5: Change in resistance with temperature

3.3 Mechanical durability of the ink⁴

Using a combination of a tensile tester and a source meter unit, we studied the resistance change

⁴ Section 3.3 has been taken from the paper “A Highly Deformable Conductive Ink for Printed Antennas and Interconnects: Silver/Fluoropolymer Composite Amalgamated by Triethanolamine” to be submitted to *Flexible and Printed Electronics*

of printed traces during multiple stretch-release cycles. To attain the superior operation of the stretchable and flexible devices, printed pattern must maintain their well performance characteristics upon stretching, bending or twisting and retain firm adhesion with the substrates. Here all the samples were heated at 110°C for 30 minutes to remove the excess solvent before stretching. In each cycle, the printed film (shown in fig. 3.5) was stretched to 110% strain at a crosshead speed of 10 mm/min, and then the strain was released at the same speed.

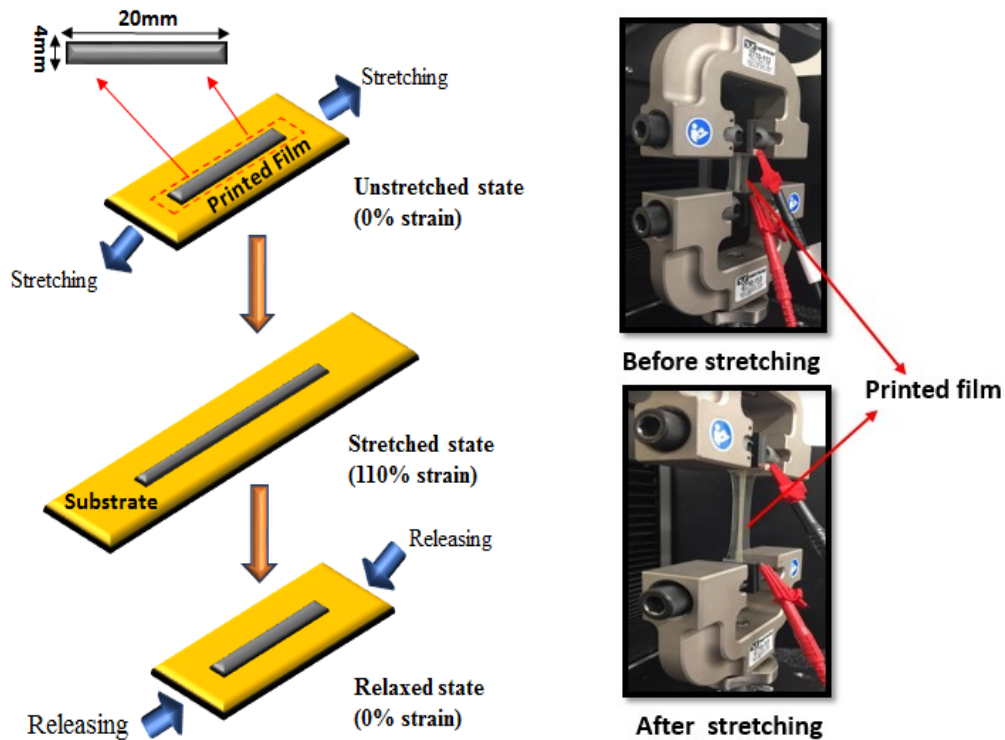


Figure 3.6: Schematic drawing for the uniaxial stretching and releasing cycle and corresponding pictures of our experimental setup

This stretch-release cycle was repeated four times (Fig 3.6(a, b)) confirms that there was very little change in resistance between each cycle due to the breakage of interconnections between the silver flakes in the composite ink, which is commonly observed on elastomer substrates.

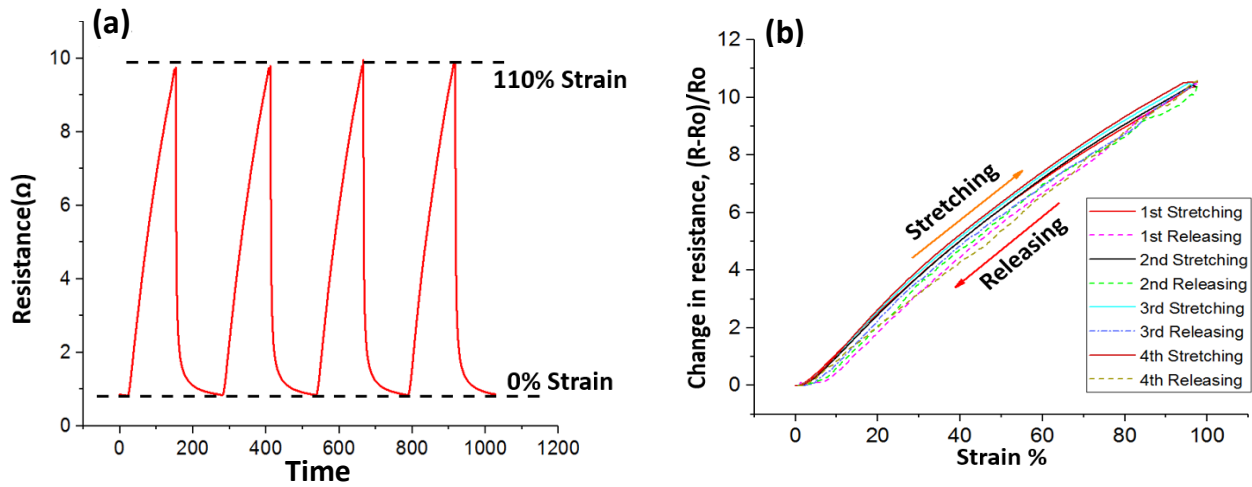


Figure 3.7: Change in resistance of the stretchable interconnect film during four stretch-release cycles. (b) Results in (a) are replotted in relative resistance versus strain curves to examine cycle to cycle variations

We also tested the change in resistance until the trace's ultimate failure at the strain value of ~500% as shown in fig 3.7. As we can see towards higher strain values, there is a rapid change in the resistance value.

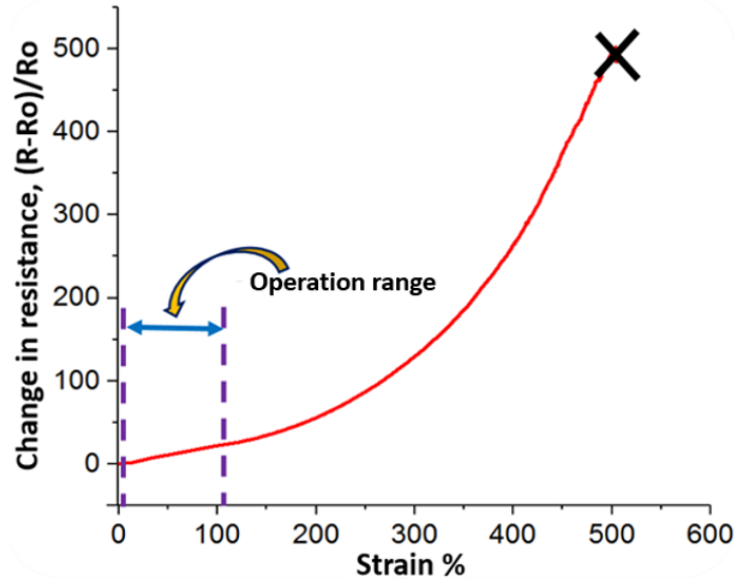


Figure 3.8: Relative resistance values with respect to strain up to the eventual failure at ~500%.

Therefore, we considered extension of 0-110% strain as “operation range” for our devices to work in a reversible manner. The comparison between the previous work and our work with conductivity value at different strain has been shown in the table 3.

Table 3: Comparison study of various elastic ink

Components	Printing method	Conductivity value at diff. Strain %	Curing temperature	Ref
Sliver- CNT composite, PVDF	Drop casting Hot rolling	5710 S/cm -0% strain 20 S/cm- 140% Strain	160° C, 12 hours	[15]
Ag/Pt embedded rGO mixed with PVDF	Screen Printing Hot Rolling	3012 S/cm- 0 % strain 322.8 S/cm – 35% strain	Room temperature, 24 hours(drying) 150°C,90 min	[11]

Ag trifluoroacetate, SIS Rubber, Butanone, DMAc(dimethylacetamide)	Printable	0.8ohm/cm – 0 % strain 20.8ohm/cm – 100% strain	Room temperature	[16]
Ag flakes (91wt%), polyurethane	Screen printable	3570 S/cm – 0% strain 1200 S/cm- 70% strain	70°C, 3 hours Low adhesion to PET/PVC	[58]
Ag flakes, MWNT, Benzyl mercaptan, Ethanol,	Wet spinning	~ 6000 S/cm – 0% strain ~260 S/cm – 70% strain	135 °C, 45 min	[59]
Ag flakes, Fluorine surfactant MIBK, Fluorine rubber	Printable	738 S/cm – 0% strain 400 S/cm- 70% strain	80 °C, 30 min	[14]
(Hydroxypropyl)methyl cellulose, fluorosurfactant, AgNW, Defoamer MO	Screen printed	46700 S/cm - 0% Strain 8002 S/cm – 70 % strain	150 °C ,30 min	[17]
Silver flakes, TEA, 4 -methyl 2 pentanone, Fluorine rubber	3D Printer	849 S/cm – 0% Strain ~100 S/cm -110%	Room temperature	Our work

3.3.1 Adhesion tests on various substrates

The ability of printed pattern to sustain deformation is a key parameter for the fabrication of flexible devices. Thus, printed structures must maintain their well- performance upon stretching, bending as well as strong adhesion with the substrates.

Here we have tested the adhesion of silver elastic ink on various substrates (PET, PDMS and VHB) by using three different methods, namely, scotch tape test, ultrasonication test and soaking test. We also want to point out that the substrates used to carry out adhesion tests were not modified in any way either chemically or through plasma treatment. As we know that these surface modifications can have significant influence on the interface bonding of the elastic ink with elastomer. However, in our case, the adhesion comes only from the adhesive nature of the ink and thus independent on the substrate. In scotch tape test, clean peeling of scotch tape from the printed

film is performed and no delamination occurs. In case of sonication test, samples were kept in ultra-sonicator for 10 minutes and observed no change in the printed film surface.

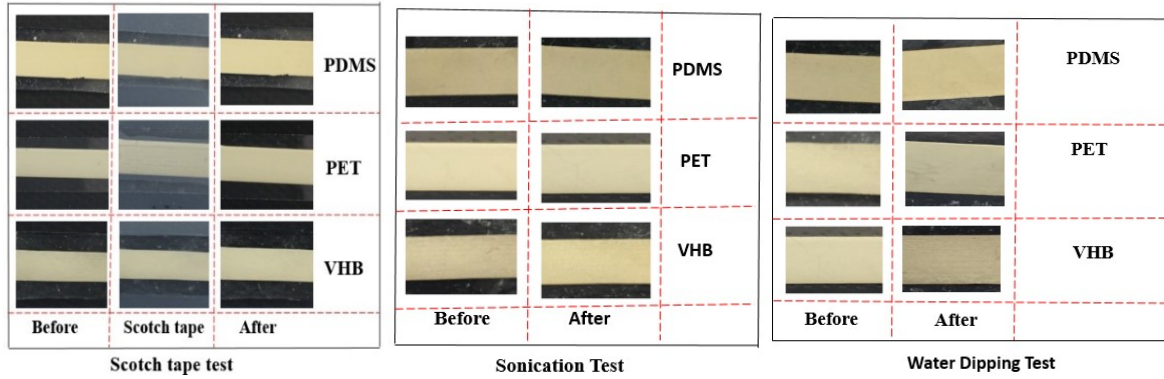


Figure 3.9: Adhesion test using different methods

In case of soaking test, samples were kept in a beaker filled with DI water for 3 hours. Since there was no case of ink delamination from any of the untreated substrates, thus, it is concluded that elastic inks adhere strongly to each of the untreated substrates and show precise, intact patterning with excellent continuity as shown in figure 3.8.

Chapter 4. Applications using elastic ink

4.1 Fabrication procedure of stretchable antennas⁵

The antennas (On-body loop, patch and bowtie) were patterned onto an elastomer (3M, VHB-4910) by using 3Dn jet printer (nScript tabletop 3Dn printer). Briefly, after the elastic ink preparation with desired viscosity, the ink is filled up in the syringe and mounted onto the printer where the positive pressure starts feeding the materials into the valve body. To start micro-dispensing, valve open and allow the material to flow smoothly through the nozzle orifice onto the substrate surface. After printing, the antennas patterns were dried at 100°C for 20min. to remove the excess solvent. The schematic of the complete process for the fabrication is shown in fig 4.1.

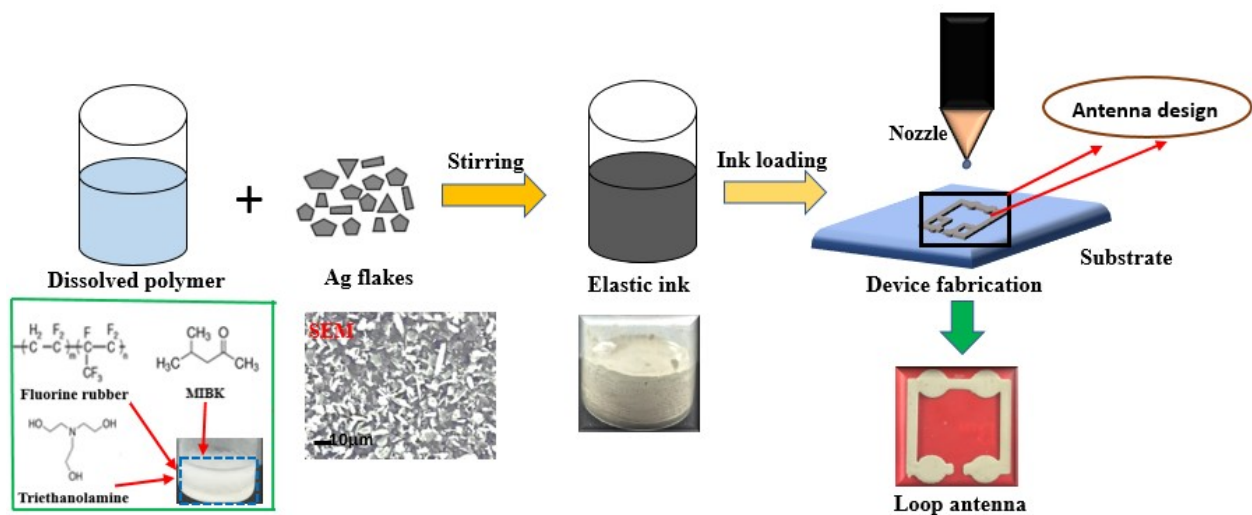


Figure 4.1: Schematics of elastic ink fabrication and the printing of stretchable traces onto elastomeric substrate for stretchable antenna fabrication.

⁵ Section 4.1 has been taken from the paper "A Highly Deformable Conductive Ink for Printed Antennas and Interconnects: Silver/Fluoropolymer Composite Amalgamated by Triethanolamine" to be submitted to *Flexible and Printed Electronics*

4.2 Conformal antenna ⁶

Three types of stretchable antennas were designed and fabricated in this work. One stretchable antenna (on-body stretchable antenna) is designed to apply on the skin of human body while the other two are targeted to wireless local area network (WLAN) for internet of things (IoT) as shown in fig 4.2(a, b). In order to convey the sensory data and provide remote diagnosis, wireless interfaces to the external communication devices are highly required and critical component for such communication is on-body antennas.

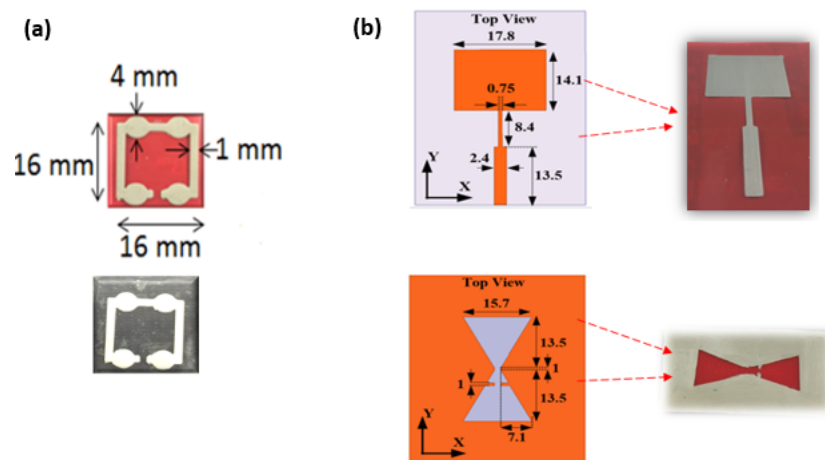


Figure 4.2: Antennas dimension (a) On-body type loop antenna (b) Patch and Bow-tie antenna. [Dimensions provided by H.A Damis and H. Saghlatoon, Device fabrication is done by Amit Kumar]

⁶ Section 4.2 has been taken from the paper “A Highly Deformable Conductive Ink for Printed Antennas and Interconnects:

Silver/Fluoropolymer Composite Amalgamated by Triethanolamine” to be submitted to *Flexible and Printed Electronics*. Simulation, antenna characterization and data interpretation in Chapter 4.2 are primarily done in Dr. Mousavi’s research group.

Two other antennas types, patch and bow-tie were also operated in a normal environment with different strain%.

4.2.1 On-body loop antenna

On-body stretchable antenna: There are a few design considerations for antennas in on-body operation. This is due to large relative permittivity of body tissues that causes significant losses of electromagnetic waves in body, and complex surface contour of body surface, while person-to-person variation of shape and body composition complicates the problem to further extent [60-62]. We attempted to have a first-order approximation model that resembles human arm to design on-body antennas by judicial simulation. Table 4 represents the parameters we employed to simulate human arm using known characteristics of body tissues and layers.

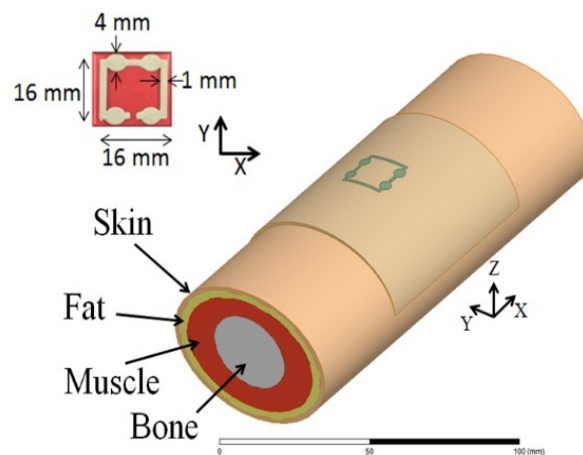


Figure 4.3: Simulation model of the on-body antenna & the arm. Reproduced with permission from [63]

Table 4: Characteristics of body tissues and layers. Reproduced with permission from [63]

Matter	ϵ_r	σ (S/m)	Tan δ
Skin	38	1.4	0.28
Fat	5.2	0.1	0.14
Muscle	52.7	1.7	0.24
Bone	18.5	0.8	0.31

The loop antenna is one of the best options for on body applications because the design's magnetic dipole performance is relatively less affected by the relative permittivity of surrounding medium compared to other antenna designs. Human body has very high relative permittivity because of its high-water content. For the on-body antenna, a square-loop structure with four circles is designed to operate at 3.5 GHz. The role of the four circles is to improve the gain and impedance bandwidth by enhancing the current distribution in the conductor path. The designed antenna structure was a 16 mm by 16 mm square and each circle is 4 mm in diameter while the thickness of the lines is 1 mm as shown in fig 4.2 (a). For the substrate, a 1 mm thick Acrylic elastomer VHB Tape 4910 (3M) with relative permittivity of 3.2 and tangent loss of 0.03 was used. As discussed earlier in the section 2.2, tangent loss value and relative permittivity are the most important parameter in selecting a substrate for antenna application. All these calculations (shown in table 4) are utilized in considering the placement of the antenna above the arm.

4.2.2 WLAN stretchable antennas

Using stretchable material and ink, reconfigurable antennas for many applications such as WLAN channels can be printed [64]. Finding new materials for stretchable antennas has been driven the

progress of the field [65-67] and the pursuit for optimal material for better performance is still in progress. Here the patch antenna and slot bow-tie antenna has been fabricated for WLAN application are shown in fig 4.4(d, g). The patch design is one of the fundamental antennas, where a ground plane is included as a separate layer that is parallel to the antenna plane, while a dielectric layer lies between the two layers. The operation frequency of a patch antenna is directly depending on the patch length, thus stretching the patch alters its resonance frequency. For the patch antenna, two-section impedance transformer has been designed to match the reflection coefficient to 50 Ohm. The bowtie slot antenna, one-side is printed by using 3D printer and the other side by screen printing technique, a wide band monolayer antenna whose shape improves the impedance of the antenna when the structure is stretched.

Vector network analyzer (VNA): For the measurement of reflection coefficient/S-parameters, vector network analyzer was used. VNA is a measurement instrument for acquiring the scattering parameters (S-parameter) of electrical networks. At RF/Microwave frequencies, measurement of the reflected and transmitted power is more convenient compared to voltages and currents which mean S-parameter measurement is more feasible than Z-, Y- and H-parameters. Although VNA is usually utilized at higher frequencies, it is possible to use it at frequencies as low as 1 Hz. The measurement results of S-parameters are shown versus frequency in VNA. According to the maximum power transfer theorem, the input impedance of the antenna should be conjugate matched to the impedance of the system. The impedance 50 Ω is set as a standard value for impedance of the RF/Microwave system [68][72]. Thus, for delivering the maximum power to the antenna, its input impedance should be 50 Ω . Since, an antenna is a one-port network only the reflection coefficient (S11) can be defined and measured for it. To test the mechanical tunability as a stretchable antenna, a tensile strain of 0-100% would be applied to it while the reflection

coefficient and radiating properties are measured using VNA, whose data should match well with the simulation results. Here, in our case, the proposed antennas are designed to operate at 3.45 GHz. As the antenna is flexible, tunable and stretchable which enable the resonant frequency to change as a function of the applied strain

4.2.3 Antennas measurement and results⁷

The simulation and measurement results of S11 in logarithmic scale for the three proposed antennas have been shown in Fig.4.4 (b), (e) and (h), respectively for different stretching lengths. The S11 graph versus frequency help in extracting the exact amount of power reflected from the antenna input port. If impedance matching occurs, then less power will be reflected and there is maximum power radiation into the space. The dB scale helps us in determining the exact value of reflected power from the input antennas port. In general, lower the value, more efficient is the antenna in accepting and radiating in space. If the value of reflection coefficient is lower than -10-dB line, i.e., more than 90% of the power is accepted by the antenna, then this value is considered as the operational bandwidth of the antenna. The frequency at which the antenna shows the higher acceptance rate in the S11 graph is considered as the resonance frequency of the antenna. In our work, when simulation was performed, it was found that the resonant frequency shifts to the lower side when the antenna was stretched to almost double of its length due to the inversely proportional relation between resonant frequency and antenna length which matches perfectly with the measurements results.

⁷ Simulation, antenna characterization and data interpretation in Chapter 4.2 are primarily done by Dr. Mousavi's research group.

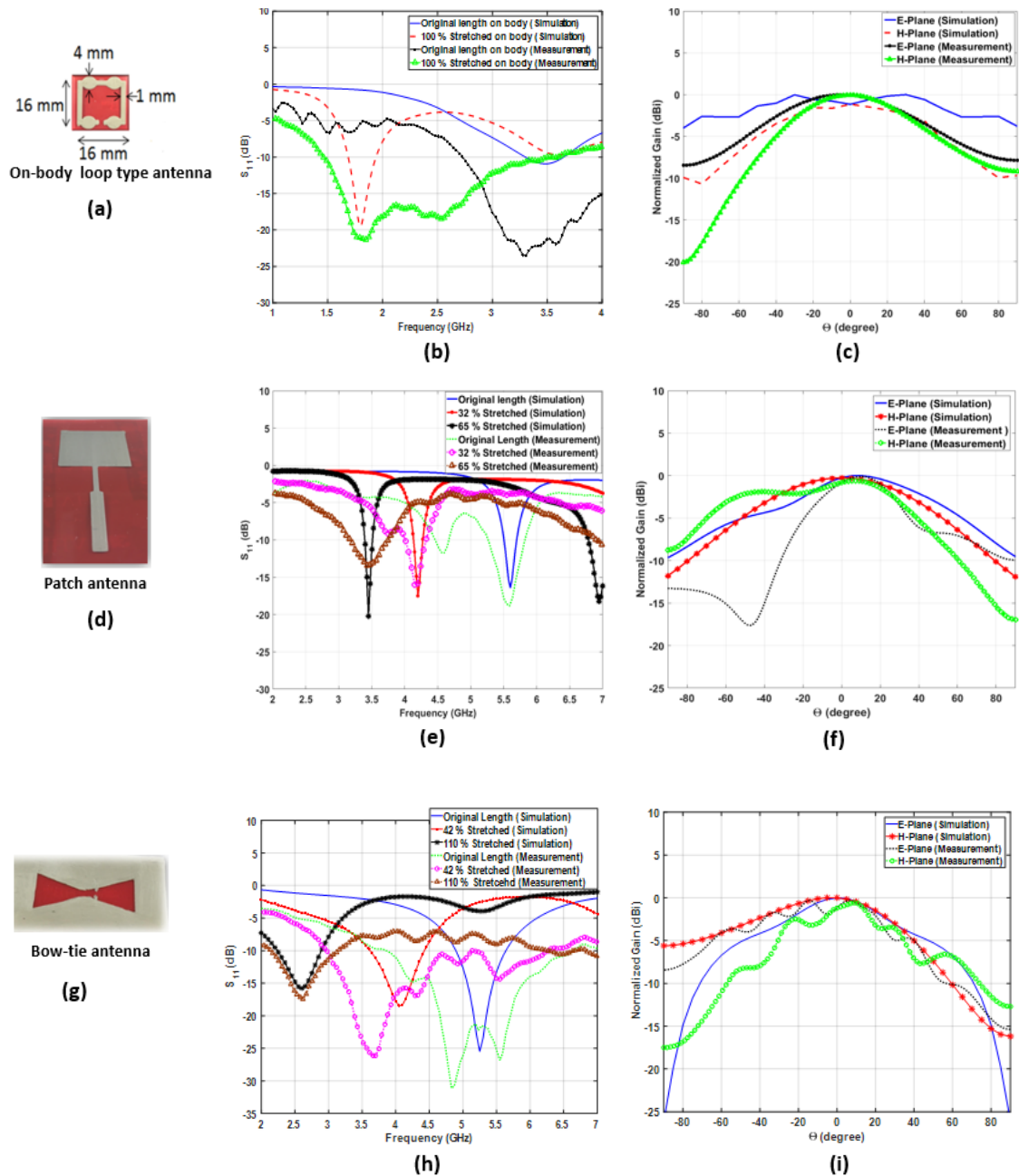


Figure 4.4: (b, e, h) Simulation and measurement results of the input reflection coefficient for different length of On-body loop, patch and bow-tie antenna. (c, f, i) normalized radiation patterns of simulation and measurements of On-body loop, patch and bow-tie antenna. [measurements were done by H. Saghlatoon and M.M.H. Kalateh]

The simulation and measurement results of the radiation patterns in E-plane and H-plane are illustrated in Fig.4.4 (c), (f) and (i). E-Plane of an antenna is the plane containing the Electric field vector which is the radiation pattern in the YZ plane. H-Plane of an antenna is the plane containing the Magnetic field vector which is the radiation pattern in the XZ plane in this paper. In addition, θ is the polar angle between Z axis and the line crossing the origin and ϕ is the azimuth angle in the XY plane between X axis and the line crossing the origin. These patterns are presented as normalized gain in dB scale for better comparisons. The radiation pattern depicts the graphical representation of the antennas radiation into the space. The higher value shows that the antenna radiates better at that specific angle, thus needs less power to communicate properly with other antennas at a certain distance.

4.2.4 Limitation of using Vector network analyzer (VNA): The limitation using such technique is noise at the measurement frequency band due to other wireless transmitter, temperature and noise of the system surroundings.



Figure 4.5: Vector Network analyzer

In order to have a proper antenna measurement, the medium should be similar to an infinite free space which means no wave should be reflected back by the boundaries in the measurement ambient and no external signal should reach the antenna from other transmitters. Therefore, an anechoic chamber is used for antenna measurements in which the walls are covered with RF/Microwave absorbers while the outer walls are shielded to insulate the inner medium. While measurements, calibration, is also one of the limitations of VNA, which is a highly complex and time consuming process. In addition, utilization of proper cables and connections is an important issue in RF/Microwave measurements.

4.3. Stretchable Heater for tunable transparent device⁸

In this work, fabrication of polyampholyte (PA) hydrogel based optically tunable window that is stretchable as well as temperature tunable is done. In brief, PA hydrogel undergoes a transition between opacity and transparency at the upper critical solution temperature (UCST). Here we demonstrated a temperature-tunable stretchable window by the combination of PA hydrogel and stretchable electric heater. The heater is fabricated with a stretchable and 3D printable elastic ink material which was initially developed in this work, using nScript 3Dn printer. To fabricate the stretchable heater, it is first printed onto the PET film due to the non-uniformity of the printing bed, which is further, transferred onto VHB elastomeric substrate as shown in fig 4.5.

⁸ Section 4.3 has been taken from the paper “Modulating Phase Transition Temperature of Tough Hydrogel Coating for Stretchable Smart Window Application” to be submitted to Advanced materials.

4.3.1 Antenna dimensions and working: It is a 2 by 2 matrix array form of an active smart window. The nozzle with diameter of 125-175 μm was used. After printing, the line resolution was measured using SEM image, which was observed around 200 μm .

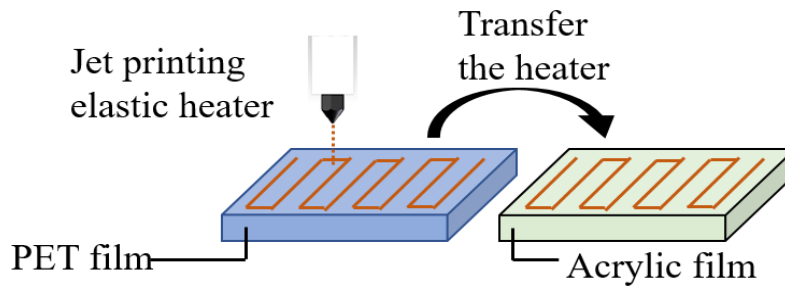


Figure 4.6: Fabrication steps of stretchable heater

To make use of stretchable heater, herein, we built an example of stretchable smart window using thin-film of PA hydrogel as shown in fig 4.8. For operation control, an elastic heater was attached to the PDMS substrate coated by the PA hydrogel thin-film. High adhesion of the acrylic elastomer and PDMS was obtained during fabrication. It is done because direct integration of the elastic heater not only offers intrinsic stretchability of the device, but also enables to control temperature of the hydrogel thin-film. Secondly, the heater is intrinsically stretchable so that its resistance change is negligible when being stretched.

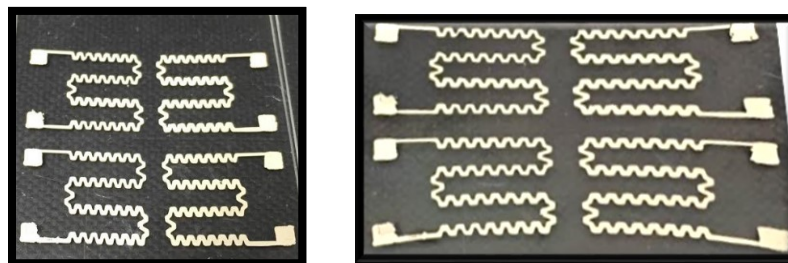


Fig 4.7: Printed heater at 0% and 80% strain on VHB. [Fabricated by T.G. La, A. Kumar]

The stretchable heater is found to be in steady-state heating even under largely mechanical deformation. Consequently, the hydrogel coating remains at stable temperature, at the same time of being stretched or wrapped. Lastly, the hydrogel-coated PDMS substrate was placed onto the heater which was printed initially onto the acrylic substrate. Thereafter, the whole device was packaged by placing another VHB acrylic membrane on top of the hydrogel which acts as ‘protective encapsulation’ against the shrinkage and drying-out of the PA hydrogel coating.

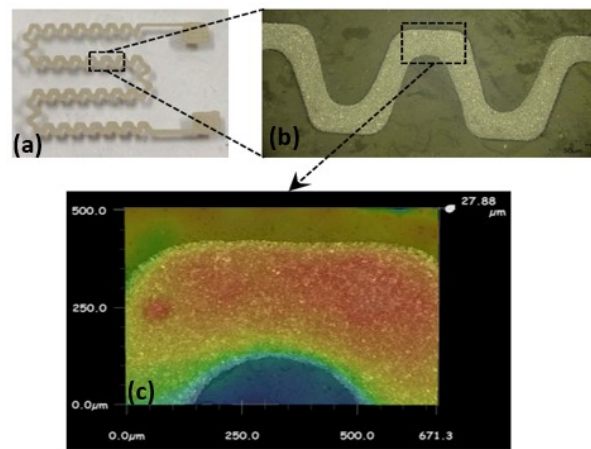


Figure 4.8: (a) Printed heater onto PET substrate (b) Microscopic image of printed heater (c) SEM image [Fabricated by T.G. La, A. Kumar]

Thereafter, a certain amount of current was allowed to flow through the device through the direct heating strategy where a hydrogel-based window can complete a cycle of heating and cooling (20°C to 60°C and reverse) in only 50 seconds (as shown in fig 4.8 a, b) in response to temperature change as shown in fig 4.8 (c).

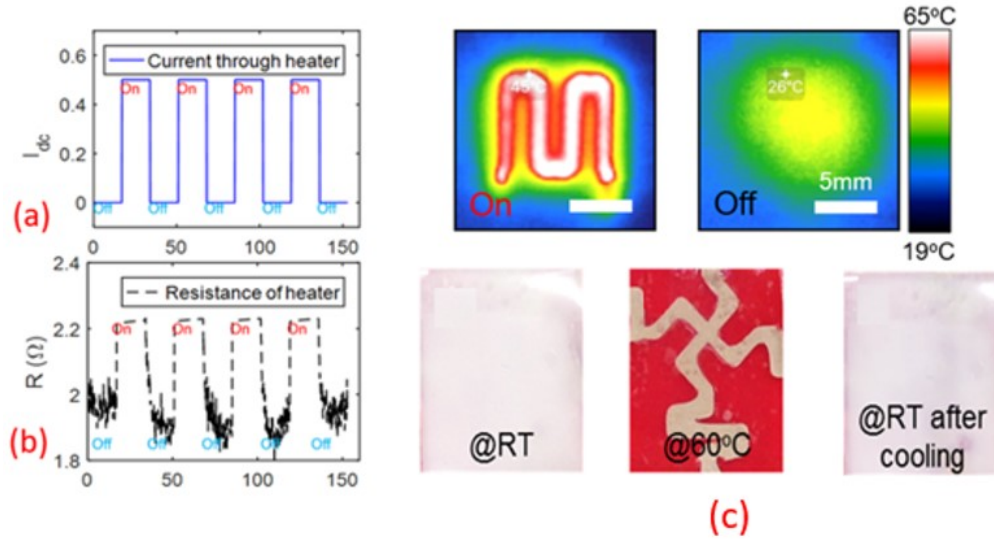


Figure 4.9: a) Applied current in cyclic process b) Resistance value in response to the applied current (c) Effect of temperature on optical properties of PA hydrogel. [Fabricated by T.G. La and A. Kumar]

Thus, the hydrogel-based window transitioned from opalescent to transparent and vice versa. In case of stretchable heater functionality, the resistance exponentially increased 80 times higher than the original value when the heater was uniaxially stretching from 0 to 200% strain.

Chapter 5. Conclusion

This work attempts to develop a novel synthesis formula for highly deformable conducting traces, where TEA is used as a compatibilizer and a plasticizer for the composite of fluoropolymer and Ag flakes. In chapter 1, we have described, in brief, about the different fabrication methods to demonstrate the functioning of several stretchable electronics devices such as reduction, meandering shape and composite based inks methods along with their challenges, drawbacks in their technique and novelty in our work. We also mentioned about the distinct types of 3D printing technique and their basic working principle.

Specifically, in chapter 2, we have described about the synthesis procedure of a novel and simple fabrication procedure for the development of 3D printable, highly conductive composite ink for the direct writing of stretchable circuits and patterns. Here we also discussed the role of TEA in the ink solution and in the printed traces which ensures a uniform dispersion of Ag flakes (filler) in the matrix of fluorine rubber and also act as a plasticizer for the polymer network, which bestows high stretchability to the conductive composite. We have also discussed about the 3D printing operation and how it works while ejecting the droplet onto the heated substrate. The droplet behaviour after impact has also been discussed in the same chapter.

In chapter 3, measurement of physicochemical and mechanical properties of the ink has been performed. Physicochemical properties include ink viscosity, thermogravimetric analysis of elastic ink and its components, conductivity variation with flakes loading and temperature effect on resistance, whereas mechanical properties include stretchability over repeated cycles and adhesion

tests on various substrates. The measured viscosity was in the range of 0.3Pa-s to 0.9Pa-s for printing. It shows excellent conductivity value because of the silver flakes and TEA interaction within the dissolved polymer matrix. Repeated extension of 110% strain was achieved easily without deteriorating the device performance with no major change in the resistance value (10-15 times of its original value). The ink also shows better adherence property to number of substrates due to the introduction of an elastomeric polymer in the ink, in addition, even better stretchability after drying.

In chapter 4, we fabricated 3.2GHz on-body loop, patch and bowtie antennas and measured their specific characteristics such as reflection coefficient and radiation pattern before and after stretching. It was observed that there is shift in the resonant frequency of antennas, when the antennas are stretched to double of their original length due to the inversely proportional relation between the length and the operating frequency. In case of stretchable heater for tunable smart window applications, a coating of PA hydrogel was done whose optical properties can be tuned by raising the temperature of the overall device and it also shows better performance with repeated extension of 80% strain.

Finally, we concluded that the preparation of novel fluoropolymer based composite elastic ink is a novel and convenient procedure; ink shows excellent behavior in terms of conductivity, stretchability and adhesion to various substrates. Due to the attribution of TEA in the elastic ink, printed circuit not only have better adhesion but also the excellent stretchability after drying. The fabricated devices such as On-body loop antenna, patch antenna, bow-tie antenna and heaters, has shown excellent performance over the repeated cycle and their measurement results are well -

matched with the simulation results. These proves that our novel ink recipe can be a promising pathway towards facile antenna fabrication which can also resolve the complex fabrication procedure for the stretchable patterns and broaden the application for wearable electronics and IoT things in daily life.

Chapter 6. Future work

Future developments of such novel material and processes will allow the fabrication of numerous stretchable electronic, radio frequency and sensory devices in a simple manner while removing the complex fabrication materials and processes. Nevertheless, some opportunities for extending the scope of this thesis still remained challenges.

1. High resolution patterning of stretchable and flexible circuits

In present work, the size of silver flakes is too high to be printed through a smaller diameter nozzle. Thus, in order to improve the resolution of the printed circuits or patterns, the available option is the replacement of micro-sized silver flakes by silver nanowires.

2. Developing low cost, highly conductive and 3D printable composite based ink

Silver flakes are highly expensive for producing the cheaper electronic devices. To lower the cost of the stretchable and flexible devices, one way is to reduce the materials cost. It can be possibly done by replacing the Ag flakes with Ag coated copper flakes due to which cost required for device fabrication will reduced significantly. However, there is oxidation issue occurs with the Ag copper flakes, which is needed to be improved in the future to make a better use of them.

3. Fabrication of several stretchable and flexible electronic devices

The fabrication of various applications of flexible and stretchable electronics/devices, including strain sensors, paper based RFID, pressure and touch sensors, stretchable displays built-in circuits and organic LED array can be carried out in a single-step process.

List of references

1. Cheng, T., et al., *Stretchable Thin-Film Electrodes for Flexible Electronics with High Deformability and Stretchability*. *Advanced Materials*, 2015. **27**(22): p. 3349-3376.
2. Hussain, A.M., et al., *Metal/Polymer Based Stretchable Antenna for Constant Frequency Far-Field Communication in Wearable Electronics*. *Advanced Functional Materials*, 2015. **25**(42): p. 6565-6575.
3. Harris, K., A. Elias, and H.-J. Chung, *Flexible electronics under strain: a review of mechanical characterization and durability enhancement strategies*. *Journal of materials science*, 2016. **51**(6): p. 2771-2805.
4. Huyghe, B., et al., *Design and manufacturing of stretchable high-frequency interconnects*. *IEEE Transactions on Advanced Packaging*, 2008. **31**(4): p. 802-808.
5. Choi, W.M., et al., *Biaxially stretchable "wavy" silicon nanomembranes*. *Nano Letters*, 2007. **7**(6): p. 1655-1663.
6. Fan, J.A., et al., *Fractal design concepts for stretchable electronics*. *Nature Communications*, 2014. **5**: p. 3266.
7. Lin, K.L., J. Chae, and K. Jain, *Design and Fabrication of Large-Area, Redundant, Stretchable Interconnect Meshes Using Excimer Laser Photoablation and *In Situ* Masking*. *IEEE Transactions on Advanced Packaging*, 2010. **33**(3): p. 592-601.
8. Khang, D.-Y., J.A. Rogers, and H.H. Lee, *Mechanical Buckling: Mechanics, Metrology, and Stretchable Electronics*. *Advanced Functional Materials*, 2009. **19**(10): p. 1526-1536.
9. Xu, F. and Y. Zhu, *Highly Conductive and Stretchable Silver Nanowire Conductors*. *Advanced Materials*, 2012. **24**(37): p. 5117-5122.
10. Park, M., et al., *Highly stretchable electric circuits from a composite material of silver nanoparticles and elastomeric fibres*. *Nat Nano*, 2012. **7**(12): p. 803-809.
11. Yoon, Y., et al., *Highly Stretchable and Conductive Silver Nanoparticle Embedded Graphene Flake Electrode Prepared by In situ Dual Reduction Reaction*. *Sci Rep*, 2015. **5**: p. 14177.
12. Cheng, S., et al., *Liquid metal stretchable unbalanced loop antenna*. *Applied Physics Letters*, 2009. **94**(14): p. 144103.
13. Sekitani, T., et al., *A rubberlike stretchable active matrix using elastic conductors*. *Science*, 2008. **321**(5895): p. 1468-1472.
14. Matsuhisa, N., et al., *Printable elastic conductors with a high conductivity for electronic textile applications*. *Nature communications*, 2015. **6**.
15. Chun, K.-Y., et al., *Highly conductive, printable and stretchable composite films of carbon nanotubes and silver*. *Nat Nano*, 2010. **5**(12): p. 853-857.
16. Hu, M., et al., *Direct Pen Writing of Adhesive Particle-Free Ultrahigh Silver Salt-Loaded Composite Ink for Stretchable Circuits*. *ACS Nano*, 2016. **10**(1): p. 396-404.
17. Liang, J., K. Tong, and Q. Pei, *A Water-Based Silver-Nanowire Screen-Print Ink for the Fabrication of Stretchable Conductors and Wearable Thin-Film Transistors*. *Advanced Materials*, 2016. **28**(28): p. 5986-5996.
18. Vieira, M.G.A., et al., *Natural-based plasticizers and biopolymer films: A review*. *European Polymer Journal*, 2011. **47**(3): p. 254-263.
19. Kumar, N. and R. Tyagi, *Dimeric Surfactants: Promising Ingredients of Cosmetics and Toiletries*. *Cosmetics*, 2013. **1**(1): p. 3.
20. Mohamed, O.A., S.H. Masood, and J.L. Bhowmik, *Optimization of fused deposition modeling process parameters: a review of current research and future prospects*. *Advances in Manufacturing*, 2015. **3**(1): p. 42-53.

21. Bikas, H., P. Stavropoulos, and G. Chryssolouris, *Additive manufacturing methods and modelling approaches: a critical review*. The International Journal of Advanced Manufacturing Technology, 2016. **83**(1-4): p. 389-405.
22. Wong, K.V. and A. Hernandez, *A review of additive manufacturing*. ISRN Mechanical Engineering, 2012. **2012**.
23. Turner, B.N. and S.A. Gold, *A review of melt extrusion additive manufacturing processes: II. Materials, dimensional accuracy, and surface roughness*. Rapid Prototyping Journal, 2015. **21**(3): p. 250-261.
24. Dedoussis, V. and J. Giannatsis. *Developing competitive products using Stereolithography Rapid Prototyping tools*. in *2009 IEEE International Conference on Industrial Engineering and Engineering Management*. 2009.
25. Krebs, F.C., *Fabrication and processing of polymer solar cells: A review of printing and coating techniques*. Solar Energy Materials and Solar Cells, 2009. **93**(4): p. 394-412.
26. Choi, H.W., et al., *Recent developments and directions in printed nanomaterials*. Nanoscale, 2015. **7**(8): p. 3338-3355.
27. Ishizaki, M., et al., *Preparation of electrochromic Prussian blue nanoparticles dispersible into various solvents for realisation of printed electronics*. Green Chemistry, 2012. **14**(5): p. 1537-1544.
28. Fan, T., et al., *N-Nitrosodiethanolamine in cosmetics, lotions and shampoos*. Food and cosmetics toxicology, 1977. **15**(5): p. 423-430.
29. Farrokhi-Rad, M. and M. Ghorbani, *Electrophoretic deposition of titania nanoparticles in different alcohols: kinetics of deposition*. Journal of the American Ceramic Society, 2011. **94**(8): p. 2354-2361.
30. Farrokhi-Rad, M. and T. Shahrabi, *Effect of triethanolamine on the electrophoretic deposition of hydroxyapatite nanoparticles in isopropanol*. Ceramics International, 2013. **39**(6): p. 7007-7013.
31. Xiao, X.F. and R.F. Liu, *Effect of suspension stability on electrophoretic deposition of hydroxyapatite coatings*. Materials Letters, 2006. **60**(21): p. 2627-2632.
32. Shang, Z.B., Y. Wang, and W.J. Jin, *Triethanolamine-capped CdSe quantum dots as fluorescent sensors for reciprocal recognition of mercury (II) and iodide in aqueous solution*. Talanta, 2009. **78**(2): p. 364-369.
33. Katari, J., V.L. Colvin, and A.P. Alivisatos, *X-ray photoelectron-spectroscopy of CdSe nanocrystals with applications to studies of the nanocrystal surface*. Journal of Physical Chemistry, 1994. **98**(15): p. 4109-4117.
34. Audic, J.-L. and B. Chaufer, *Influence of plasticizers and crosslinking on the properties of biodegradable films made from sodium caseinate*. European Polymer Journal, 2005. **41**(8): p. 1934-1942.
35. Song, L., et al., *Stretchable and Reversibly Deformable Radio Frequency Antennas Based on Silver Nanowires*. ACS Applied Materials & Interfaces, 2014. **6**(6): p. 4248-4253.
36. Ramli, M.N., et al., *Dual-band wearable fluidic antenna with metasurface embedded in a PDMS substrate*. Applied Physics A, 2017. **123**(2): p. 149.
37. Khaleel, H.R., H.M. Al-Rizzo, and D.G. Rucker, *Compact polyimide-based antennas for flexible displays*. Journal of Display Technology, 2012. **8**(2): p. 91-97.
38. Rius, R.M., G. Talavera, and J. Carrabina. *Developing and study of wearable and flexible antennas for Body Area Networks working under extreme conditions*. in *2012 15 International Symposium on Antenna Technology and Applied Electromagnetics*. 2012.
39. Guo, X., et al., *Flexible and wearable 2.45 GHz CPW-fed antenna using inkjet-printing of silver nanoparticles on pet substrate*. Microwave and Optical Technology Letters, 2017. **59**(1): p. 204-208.

40. Salvado, R., et al., *Textile Materials for the Design of Wearable Antennas: A Survey*. *Sensors*, 2012. **12**(11): p. 15841.
41. Hertleer, C., et al., *A textile antenna for off-body communication integrated into protective clothing for firefighters*. *IEEE Transactions on Antennas and Propagation*, 2009. **57**(4): p. 919-925.
42. Li, B., P.A. Clark, and K. Hail. *Robust printing and dispensing solutions with three sigma volumetric control for 21st century manufacturing and packaging*. in *MRS Proceedings*. 2007. Cambridge Univ Press.
43. Singh, M., et al., *Inkjet printing—process and its applications*. *Advanced materials*, 2010. **22**(6): p. 673-685.
44. Derby, B., *Inkjet printing of functional and structural materials: fluid property requirements, feature stability, and resolution*. *Annual Review of Materials Research*, 2010. **40**: p. 395-414.
45. Goghari, A.A. and S. Chandra, *Producing droplets smaller than the nozzle diameter by using a pneumatic drop-on-demand droplet generator*. *Experiments in Fluids*, 2008. **44**(1): p. 105-114.
46. Deegan, R.D., et al., *Capillary flow as the cause of ring stains from dried liquid drops*. *Nature*, 1997. **389**(6653): p. 827-829.
47. Duineveld, P.C., *The stability of ink-jet printed lines of liquid with zero receding contact angle on a homogeneous substrate*. *Journal of Fluid Mechanics*, 2003. **477**: p. 175-200.
48. Magdassi, S., *Ink requirements and formulations guidelines*. *The chemistry of inkjet inks*. New Jersey-London-Singapore: World Scientific, 2010: p. 19-41.
49. Pond, S.F., *Inkjet technology and product development strategies*. 2000.
50. de Gans, B.J., P.C. Duineveld, and U.S. Schubert, *Inkjet printing of polymers: state of the art and future developments*. *Advanced materials*, 2004. **16**(3): p. 203-213.
51. Smith, P.J., et al., *Inkjet-based micromanufacturing*. Vol. 9. 2012: John Wiley & Sons.
52. Reis, N. and B. Derby. *Ink jet deposition of ceramic suspensions: Modeling and experiments of droplet formation*. in *MRS proceedings*. 2000. Cambridge Univ Press.
53. Duineveld, P.C., et al. *Ink-jet printing of polymer light-emitting devices*. in *International Symposium on Optical Science and Technology*. 2002. International Society for Optics and Photonics.
54. Lim, J.A., et al., *Self-Organization of Ink-jet-Printed Triisopropylsilylethynyl Pentacene via Evaporation-Induced Flows in a Drying Droplet*. *Advanced functional materials*, 2008. **18**(2): p. 229-234.
55. Park, J. and J. Moon, *Control of colloidal particle deposit patterns within picoliter droplets ejected by ink-jet printing*. *langmuir*, 2006. **22**(8): p. 3506-3513.
56. Derby, B. and N. Reis, *Inkjet printing of highly loaded particulate suspensions*. *MRS bulletin*, 2003. **28**(11): p. 815-818.
57. National Center for Biotechnology Information. *PubChem Compound Database*; CID=7618, <https://pubchem.ncbi.nlm.nih.gov/compound/7618> (accessed May 2, 2017).
58. Araki, T., et al., *Printable and stretchable conductive wirings comprising silver flakes and elastomers*. *IEEE Electron Device Letters*, 2011. **32**(10): p. 1424-1426.
59. Ma, R., et al., *Knitted fabrics made from highly conductive stretchable fibers*. *Nano letters*, 2014. **14**(4): p. 1944-1951.
60. Li, X., et al., *A compact double-layer on-body matched bowtie antenna for medical diagnosis*. *IEEE Transactions on Antennas and Propagation*, 2014. **62**(4): p. 1808-1816.
61. Xu, L.-J., et al., *A Dual-Band On-Body Repeater Antenna for Body Sensor Network*. *IEEE Antennas and Wireless Propagation Letters*, 2016. **15**: p. 1649-1652.
62. Agarwal, K., Y.-X. Guo, and B. Salam, *Wearable AMC backed near-endfire antenna for on-body communications on latex substrate*. *IEEE Transactions on Components, Packaging and Manufacturing Technology*, 2016. **6**(3): p. 346-358.

63. Damis, H.A., et al. *Flexible printed square loop antennas for wearable applications*. in *2016 17th International Symposium on Antenna Technology and Applied Electromagnetics (ANTEM)*. 2016.
64. Rai, T., et al., *A stretchable RF antenna with silver nanowires*. *IEEE Electron Device Letters*, 2013. **34**(4): p. 544-546.
65. Nakano, H., et al., *Slot bowtie antenna for dual-frequency operation*. *Electronics Letters*, 2007. **43**(10): p. 554-555.
66. Kiourti, A. and J.L. Volakis, *Stretchable and flexible E-fiber wire antennas embedded in polymer*. *IEEE Antennas and Wireless Propagation Letters*, 2014. **13**: p. 1381-1384.
67. Liyakath, R.A., A. Takshi, and G. Mumcu, *Multilayer stretchable conductors on polymer substrates for conformal and reconfigurable antennas*. *IEEE Antennas and Wireless Propagation Letters*, 2013. **12**: p. 603-606.
68. Ayasli, Y. and P.J. Katzin, *High-power rf switching system*. 1991, Google Patents.
69. nScrypt, Web.12Apr.2017
(<https://www.nscrypt.com>)
70. 3M VHB Tape 4910, Web.30 Apr. 2017
(<https://multimedia.3m.com/mws/media/9866950/3m-vhb-tape-specialty-tapes.pdf>)
71. Hild, F., *Surface energy of plastics*. Tristar, 16 Dec. 2009. Web 12 Apr.2017.
(www.tstar.com/blog/bid/33845/Surface-Energy-of-Plastics)
72. Engdahl, T; *Impedance and impedance matching*. epanorma.net, 20 Feb.2016. Web.30 Apr.2017
(<http://www.epanorama.net/newepa/2016/02/20/impedance-and-impedance-matching>)

Appendix 1 – Supplementary Data

Drop coalescence and Stability: To develop a continuous feature, overlapping of drops will occur and formation of beads takes place. Duenveld et.al [47] studied the stability of fluids/beads on the flat and smooth surface at certain conditions. In the first case, the contact angle was fixed at the line but the contact line is free to move. The contact angle was considered as function of contact line with zero line speed and the contact angle can be changed but this time the radius of the fluid was kept fixed. In such kind of printing, bead formation takes place only due to the overlapping of adjacent drop spreading. If the overlapping between drops doesn't occurs, then it leads to non-formation of the beads. When there is occurrence of contact line pinning, then the two overlapping drops will coalesce, and allow to form a continuous flow. In the experiments, they explored the liquid drop behavior on number of substrates with different contact angles and observed three regimes. If there is no change in the contact angle to the substrate, then line is found to be unstable. But in case, if the hysteresis occurs in the contact angle of the liquid drop, stability can be achieved at low value of the receding angle. Thus, instability can be observed, when a new deposited drop interacts with the leading edge of the liquid bead. They found that there is maximum stable liquid bead width using inkjet printing and considered how a stable liquid bead is formed through droplet overlapping. At low contact angle, the bead can be considered as a segment of sphere which is defined by the contact angle. The width of the liquid bead is given by

$$w = \sqrt{\frac{2\Pi d_0^3}{3p\left(\frac{\Theta^*}{\sin^2\Theta^*} - \frac{\cos\Theta^*}{\sin\Theta^*}\right)}}$$

Where p is the drop spacing, Θ is the static advancing angle.

There will be minimum width of line at threshold but as the spacing between the droplets decreases, leads to the formation of thicker beads.